AD-776 046

NEAR FIELD SMALL EARTHQUAKE--COMPUTER SIMULATION

J. Theodore Cherry

Systems, Science and Software

Prepared for:

Air Force Office of Scientific Research

30 January 1974

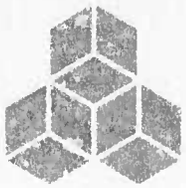

SYSTEMS, SCIENCE AND SOFTWARE

SSS-R-74-2072

NEAR FIELD SMALL EARTHQUAKE--COMPUTER SIMULATION

Semiannual Technical Report
For Period 1 June - 31 December 1973

Project Manager: J. Theodore Cherry (714) 453-0060

Sponsored by
Air Force Office of Scientific Research
Arlington, Virginia 22209

ARPA Order No. 2134

Program Code 2F10
Contract No. F44620-72-C-0051
Effective Date of Contract: 1 June 1972
Contract Completion Date: 30 June 1974 S^3 Project 195

January 30, 1974

P.O. BOX 1620, LA JOLLA, CALIFORNIA 92037, TELEPHONE (714) 453-0060

UNCLASSIFIED

SECURITY CLASSIFICATION OF THIS PAGE (When Data Entered)

AD-776046

REPORT DOCUMENTATION PAGE

READ INSTRUCTIONS BEFORE COMPLETING FORM

1. REPORT NUMBER: AFOSR - TR-74-0358	2. GOVT ACCESSION NO.
3. RECIPIENT'S CATALOG NUMBER	
4. TITLE (and Subtitle): Near Field Small Earthquake - Computer Simulation	5. TYPE OF REPORT & PERIOD COVERED: Interim 1 Jun-31 Dec 73
6. PERFORMING ORG. REPORT NUMBER: SSS-R-74-2072	
7. AUTHOR(s): Dr. J. Theodore Cherry	8. CONTRACT OR GRANT NUMBER(s): F44620-72-C-0051
9. PERFORMING ORGANIZATION NAME AND ADDRESS: Systems, Science and Software, PO Box 1620, La Jolla, CA 92037	10. PROGRAM ELEMENT, PROJECT, TASK AREA & WORK UNIT NUMBERS: 62701E; AO 2134
11. CONTROLLING OFFICE NAME AND ADDRESS: Advanced Research Projects Agency/NMR, 1400 Wilson Boulevard, Arlington, VA 22209	12. REPORT DATE: 30 Jan 74
	13. NUMBER OF PAGES: 50
14. MONITORING AGENCY NAME & ADDRESS (if different from Controlling Office): Air Force Office of Scientific Research/NP, 1400 Wilson Boulevard, Arlington, VA 22209	15. SECURITY CLASS. (of this report): UNCLASSIFIED
	15a. DECLASSIFICATION/DOWNGRADING SCHEDULE

16. DISTRIBUTION STATEMENT (of this Report)

Approved for public release; distribution unlimited.

17. DISTRIBUTION STATEMENT (of the abstract entered in Block 20, if different from Report)

18. SUPPLEMENTARY NOTES

19. KEY WORDS (Continue on reverse side if necessary and identify by block number)

Teleseismic ground motion
Earthquakes
Nuclear Explosions
Predictave Capability

20. ABSTRACT (Continue on reverse side if necessary and identify by block number)

The capability to predict and understand discriminatory features of teleseismic ground motion from earthquakes and nuclear explosions is close at hand. A complete predictive capability now exists for estimating body wave and surface wave teleseismic ground motion caused by an explosive source as a function of depth of burial, near-source environment, and earth structure. These advances in the explosion ground motion prediction are are by and large due to a realistic calculation of the explosion equivalent elastic source, based on a specification of the rock properties at the source, and the ability to propagate this source

DD FORM 1 JAN 73 1473 EDITION OF NOV 65 IS OBSOLETE

UNCLASSIFIED

SECURITY CLASSIFICATION OF THIS PAGE (When Data Entered)

20 cont'd - to teleseismic distances through a given earth structure. A similar predictive capability for earthquakes will exist when the equivalent elastic source for an earthquake is determined. Therefore, the central question may be stated as follows: Is it possible to develop an earthquake model, whose parameters may be obtained from laboratory tests on rock samples, that is capable of specifying the earthquake's equivalent elastic source? Our results to date indicate that the answer to this question should be affirmative. The approach we have taken has involved incorporating a stick-slip rupture model into a two-dimentional (plane strain) Lagrangian stress wave code. This earthquake model now furnishes the near source (free-field and free surface) ground motion caused by the stick-slip rupture process.

I. INTRODUCTION

The capability to predict and therefore understand the discriminatory features of teleseismic ground motion from earthquakes and nuclear explosions is close at hand. A complete predictive capability now exists for estimating body wave and surface wave teleseismic ground motion caused by an explosive source as a function of depth of burial, near-source environment, and earth structure (Cherry, et al., 1973). These advances in the explosion ground motion prediction area are by and large due to a realistic calculation of the explosion equivalent elastic source, based on a specification of the rock properties at the source, and the ability to propagate this source to teleseismic distances through a given earth structure.

A similar predictive capability for earthquakes will exist when the equivalent elastic source for an earthquake is determined. Therefore, the central question may be stated as follows: Is it possible to develop an earthquake model, whose parameters may be obtained from laboratory tests on rock samples, that is capable of specifying the earthquake's equivalent elastic source?

Our results to date indicate that the answer to this question should be affirmative. The approach we have taken has involved incorporating a stick-slip rupture model into a two-dimentional (plane strain) Lagrangian stress wave code. This earthquake model now furnishes the near source (free-field and free surface) ground motion caused by the stick-slip rupture process.

A description of the model along with free field theoretical seismograms, radiation patterns and displacement spectra for various fault lengths, rupture velocities and dynamic stress drops have been given by Cherry (1973) and we assume the reader is familiar with that report. We have used the model to simulate the February 9, 1971 San Fernando earthquake. Theoretical results for that earthquake are presented in Section II and compared with the recorded ground motion at Pacoima Dam. In Section III we investigate the "far field" nature of the displacement spectrum, where in this case far field corresponds to ground motion five fault dimensions away from the source.

II. FREE SURFACE EARTHQUAKE GROUND MOTION

Two thrust fault calculations were run with the only variable being the dip of the fault. The fault length for each calculation was 5 km and the dynamic stress drop was 0.5 kbar. A homogeneous geologic environment was assumed with a P-wave velocity of 5.7 km/sec and an S-wave velocity of 3.4 km/sec.

Figure 1 is a schematic of the calculation (T-45) in which a 45° dip was assumed for the fault. The focal depth was 11.67 km. The average rupture velocity was 3.1 km/sec as shown in Fig. 2. The maximum relative displacement across the fault was 5.86 meters and occurred 4.5 km from the focus (Fig. 3).

Free surface ground motion was monitored at various distances from the epicenter. Figures 4 through 15 give the vertical ($\dot{x}$) and horizontal ($\dot{y}$) components of particle velocity at the indicated epicentral distances with the origin of the coordinate system at the epicenter (Fig. 1). In the region between the fault trace and the epicenter, the horizontal component of particle velocity is always a maximum towards the epicenter while the vertical component has its largest value in the up direction.

Figure 16 is a schematic of the calculation (T-90) which assumed a 90° dip for the fault. The focal depth was 16.5 km. Both the rupture velocity and relative displacement across the fault were the same as the T-45 calculation and are given in Figs. 2 and 3.

Figures 17 through 28 give the vertical ($\dot{x}$) and horizontal ($\dot{y}$) components of particle velocity at the indicated epicentral distances for the vertical fault.

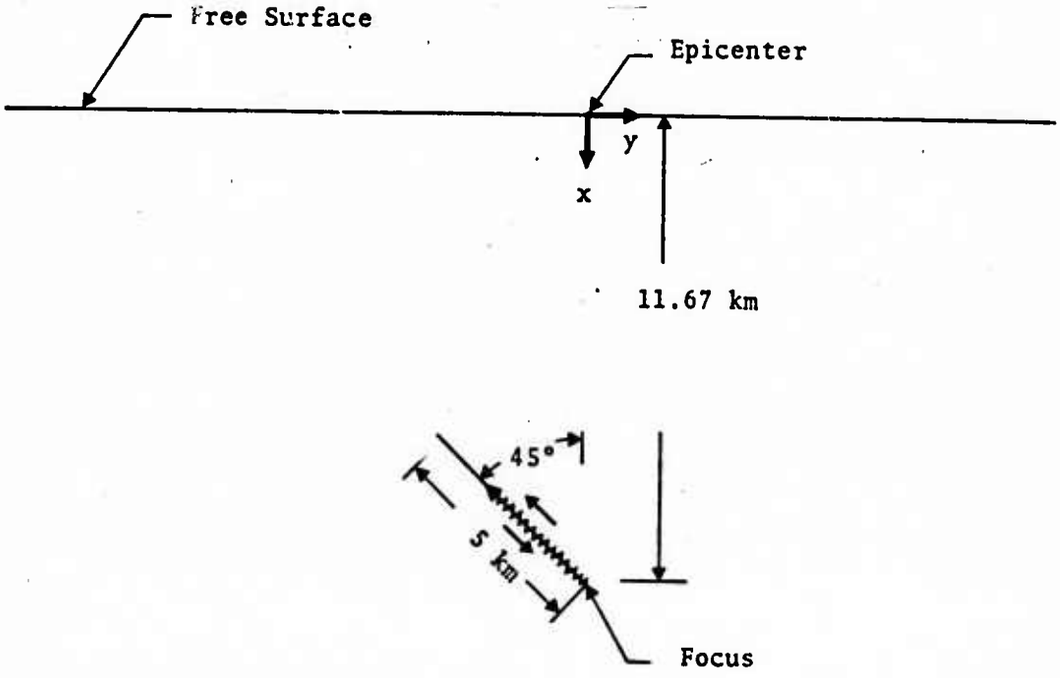

Fig. 1--Schematic of Calculation T-45. The focal depth was 11.67 km and the rupture length was 5 km. The stations monitored were at the free surface, between the epicenter and the fault zone.

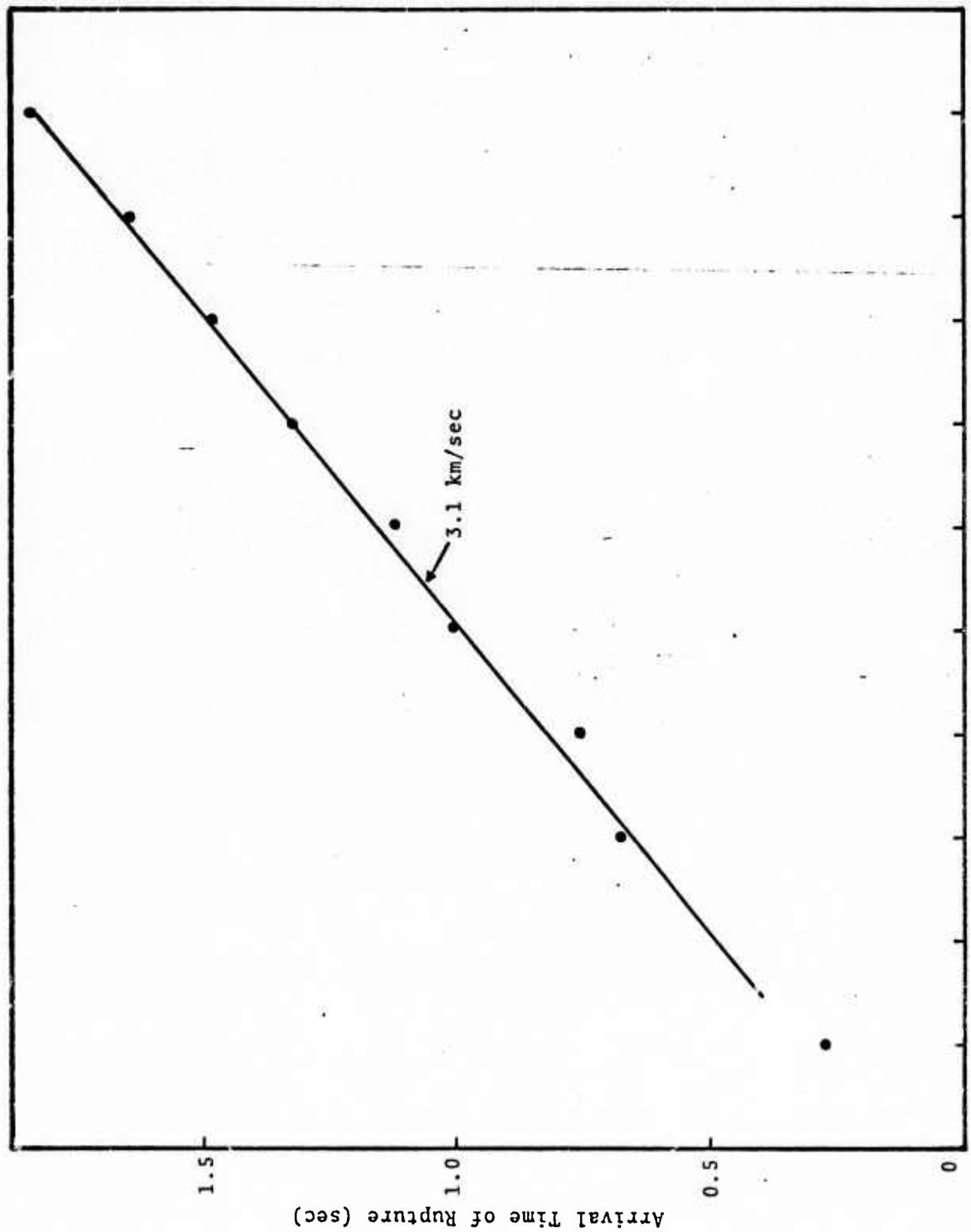

Fig. 2--Rupture arrival time versus distance along the fault for T-45 and T-90 calculations.

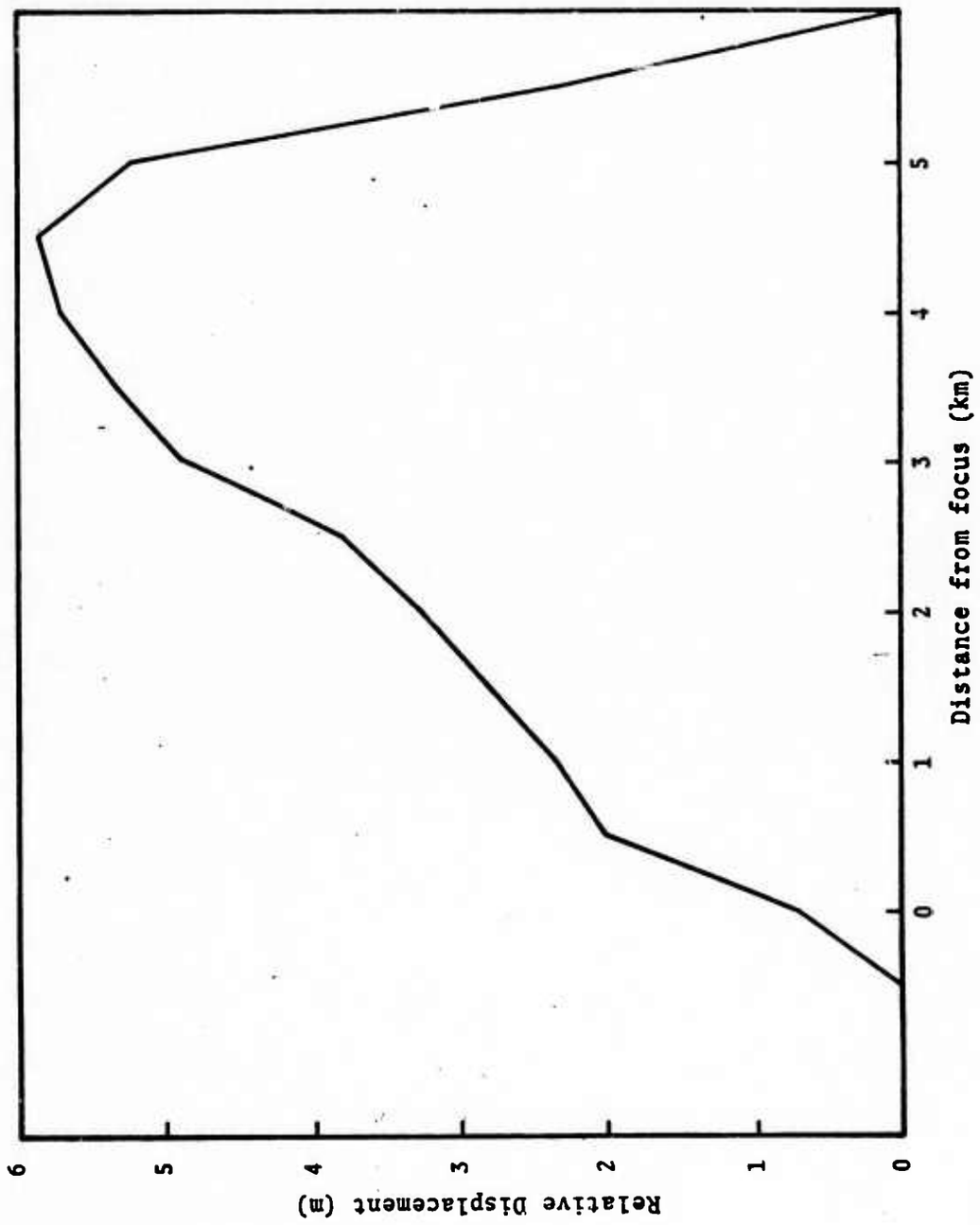

Fig. 3--Final relative displacement across the fault for T-45 and T-90 calculations. The maximum displacement is 5.86 m and occurs 4.5 km from the focus.

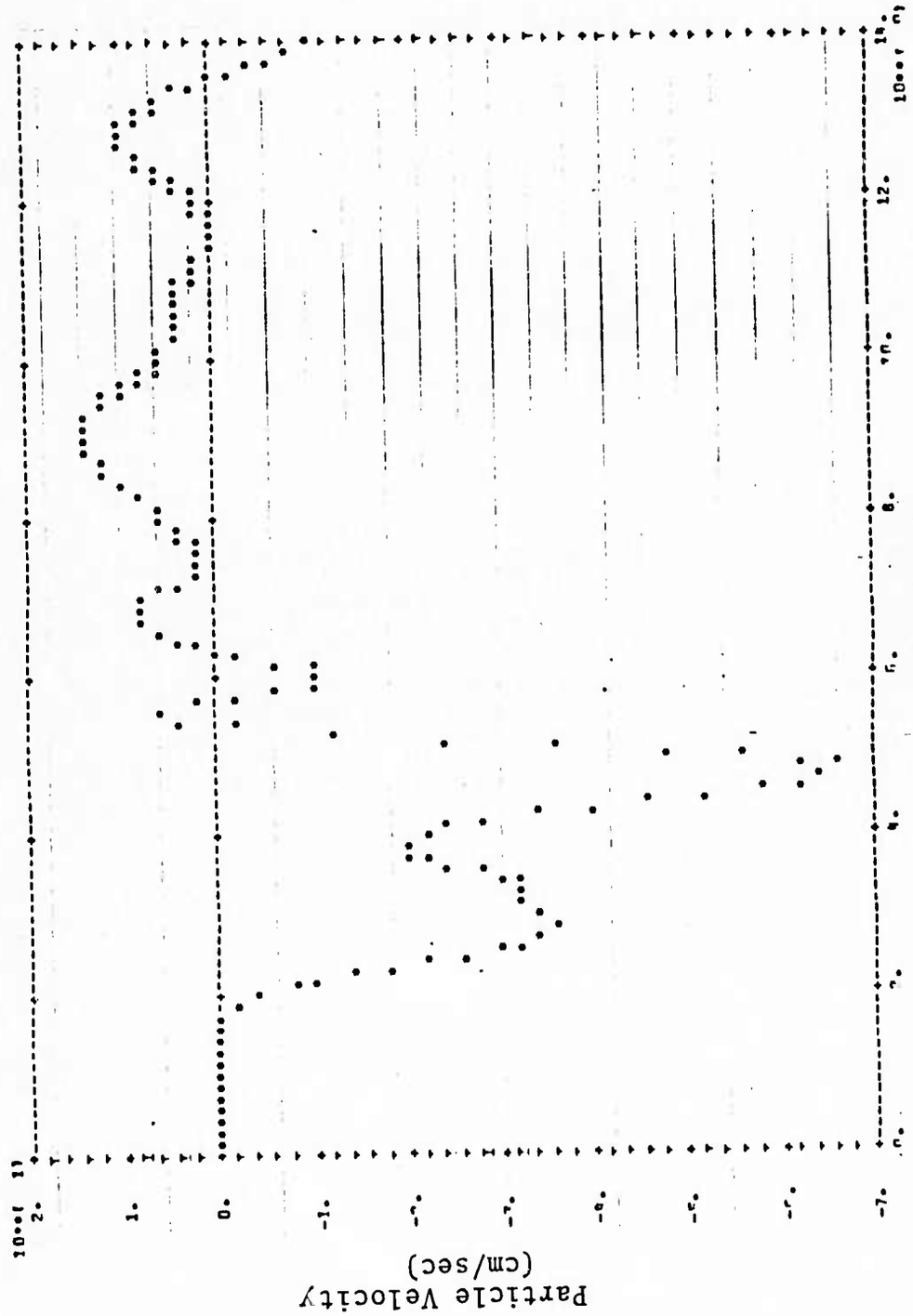

Fig. 4--Vertical component of particle velocity at x = 0, y = -1.67 km for Calculation T-45.

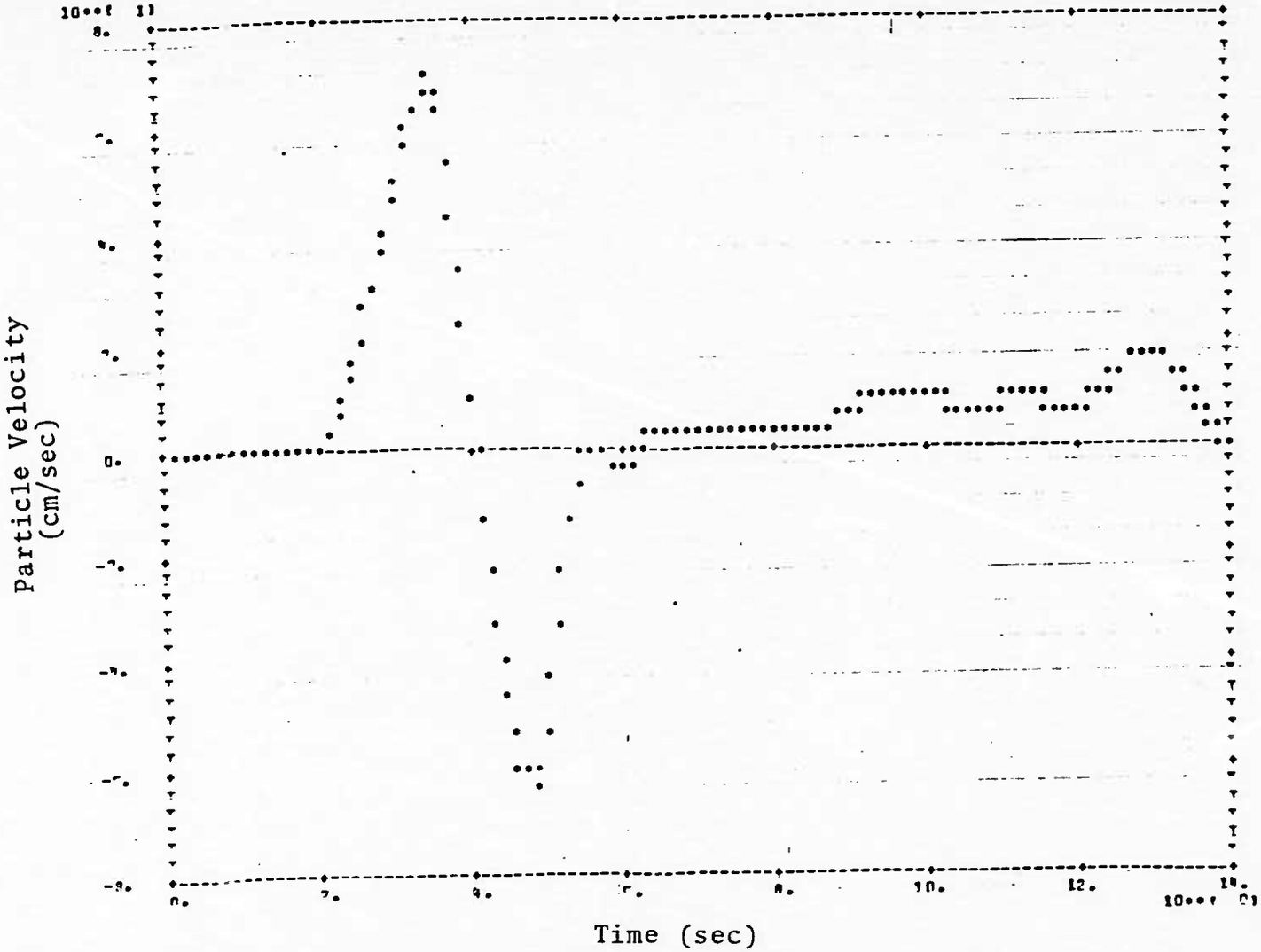

Fig. 5--Horizontal component of particle velocity at x = 0, y = 1.67 km for Calculation T-45.

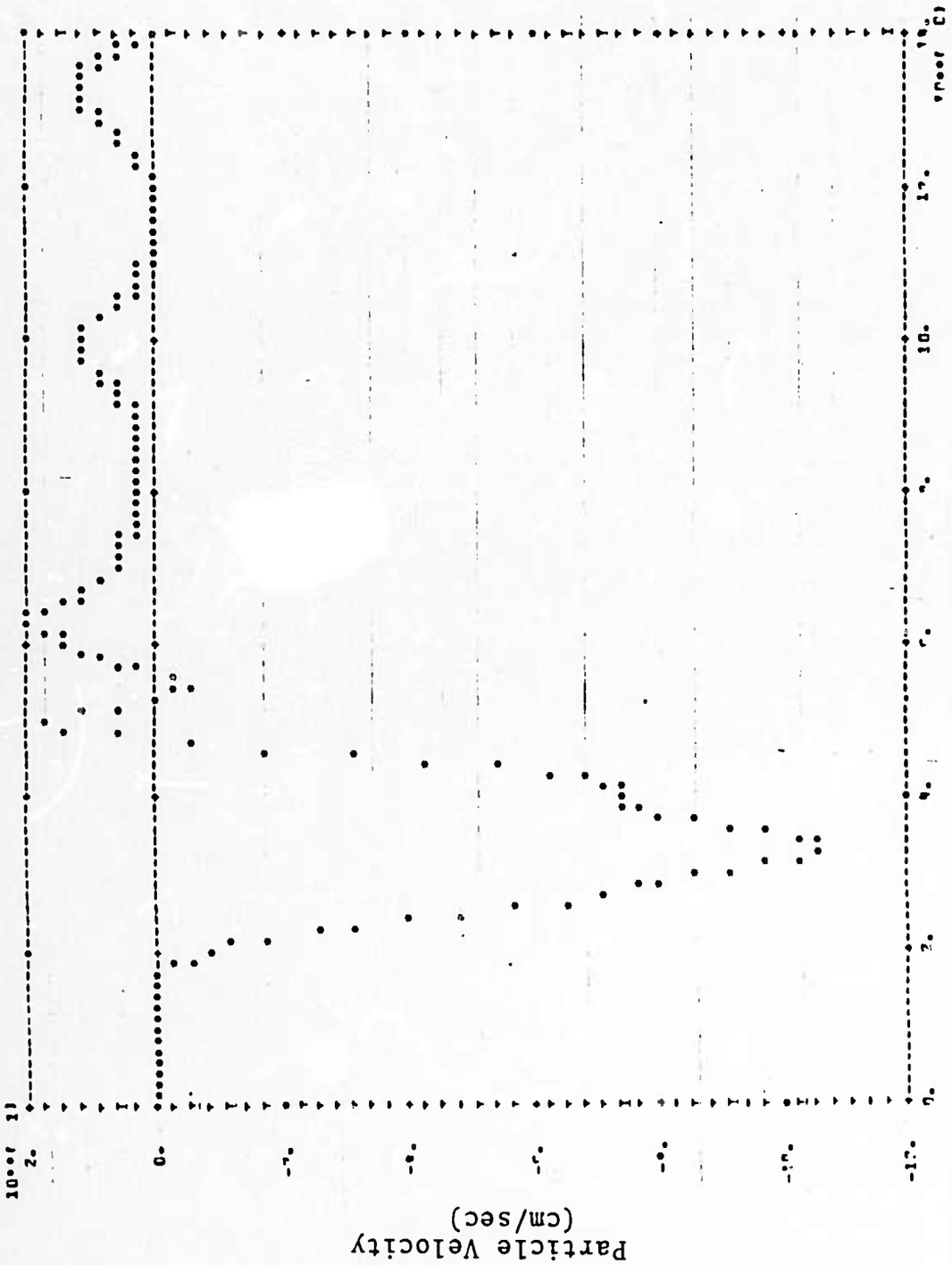

Fig. 6--Vertical component of particle velocity at x = 0, y = 3.67 km for Calculation T-45.

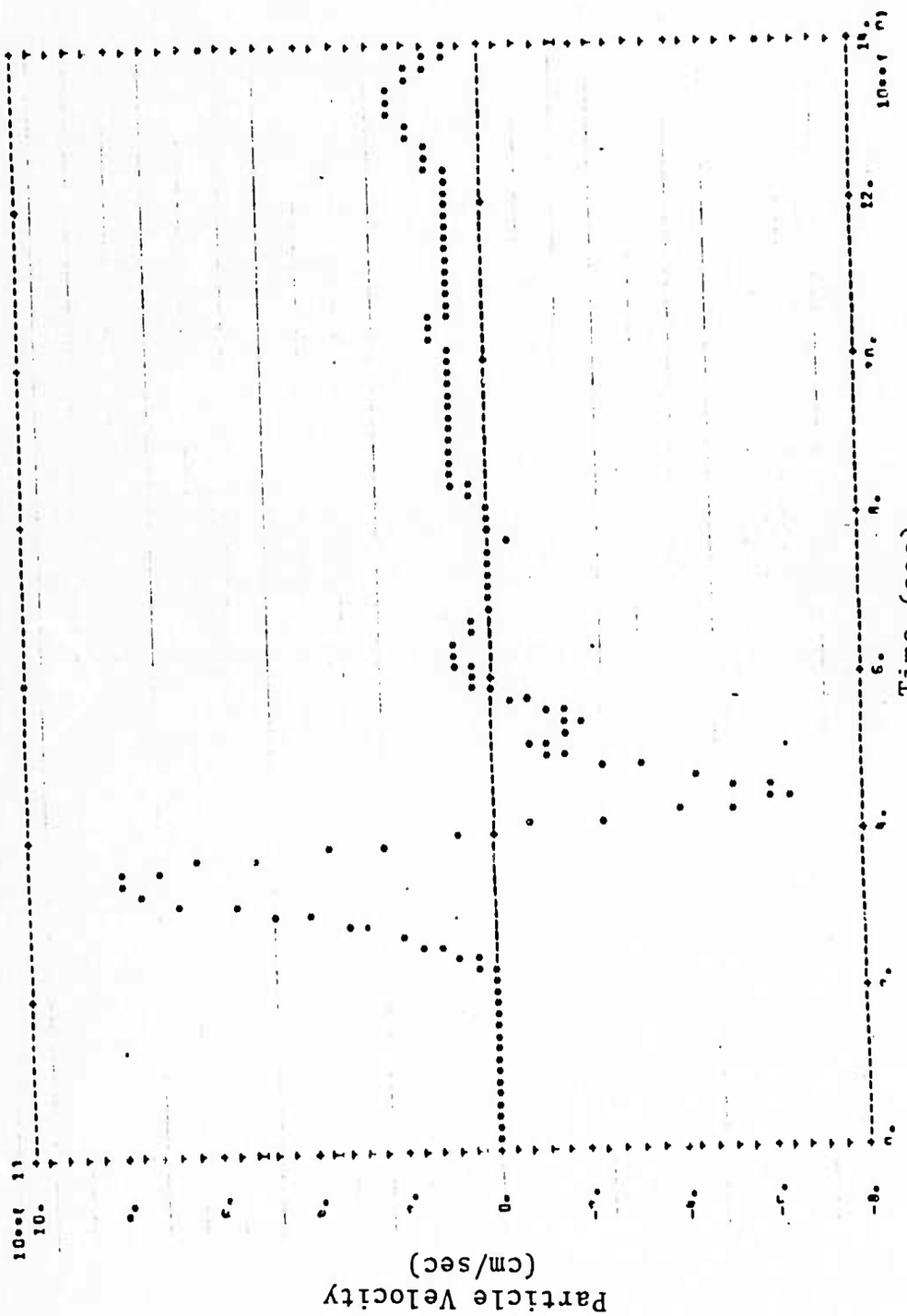

Fig. 7--Horizontal component of particle velocity at x = 0, y = 3.67 km for Calculation T-45.

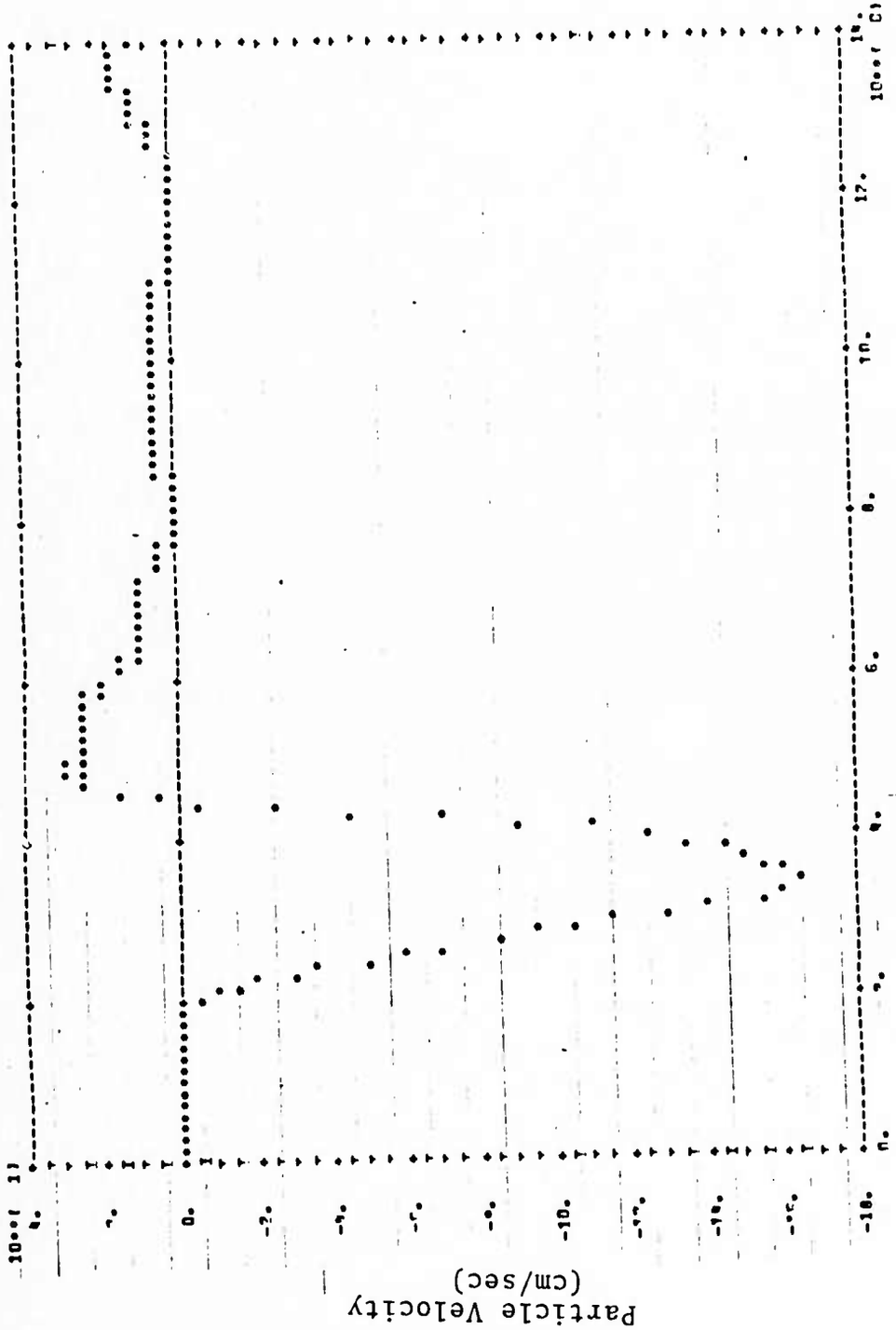

Fig. 8--Horizontal component of particle velocity at x = 0, y = -5.67 km for Calculation T-45.

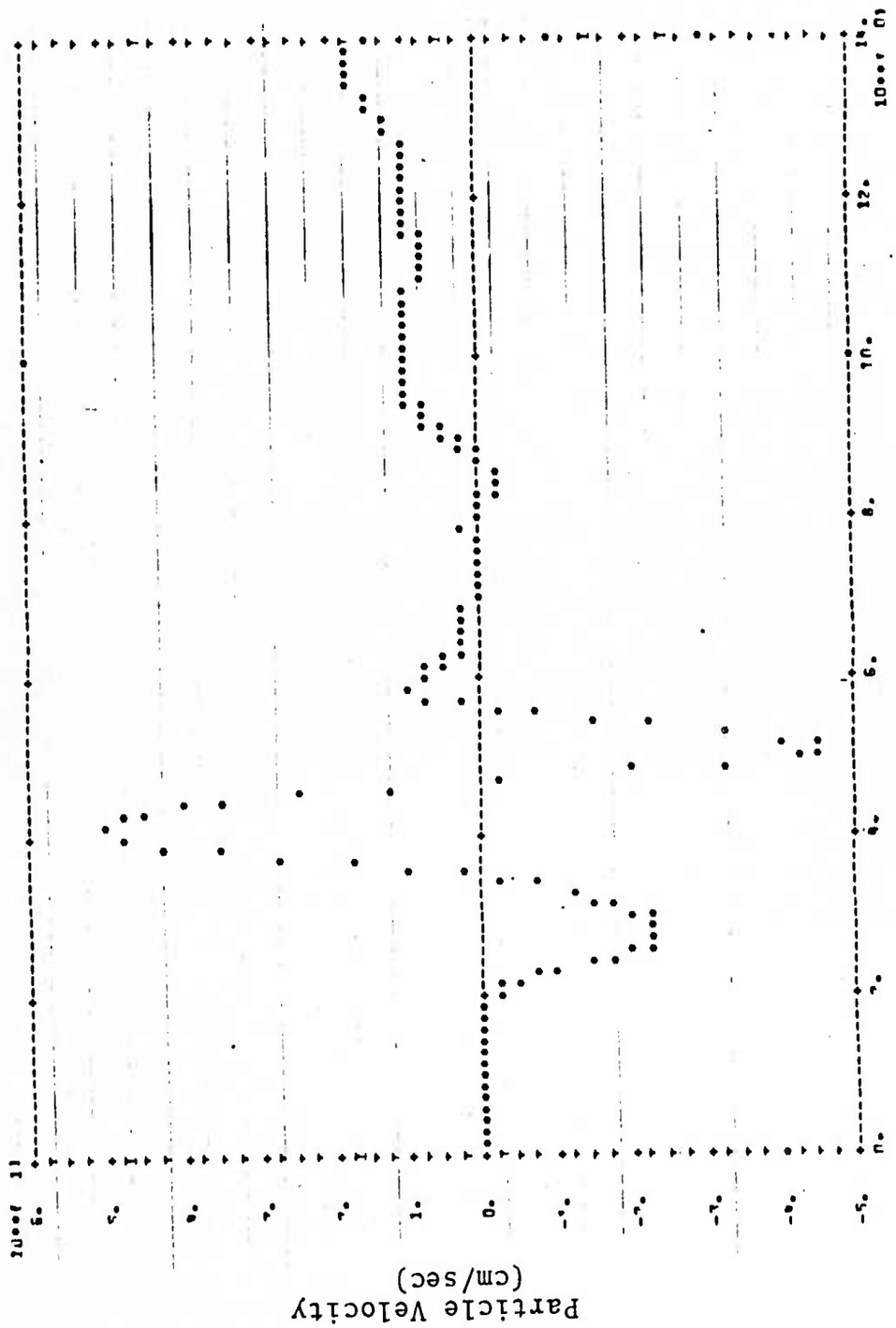

Fig. 9--Vertical component of particle velocity at x = 0, y = -5.67 km for Calculation T-45.

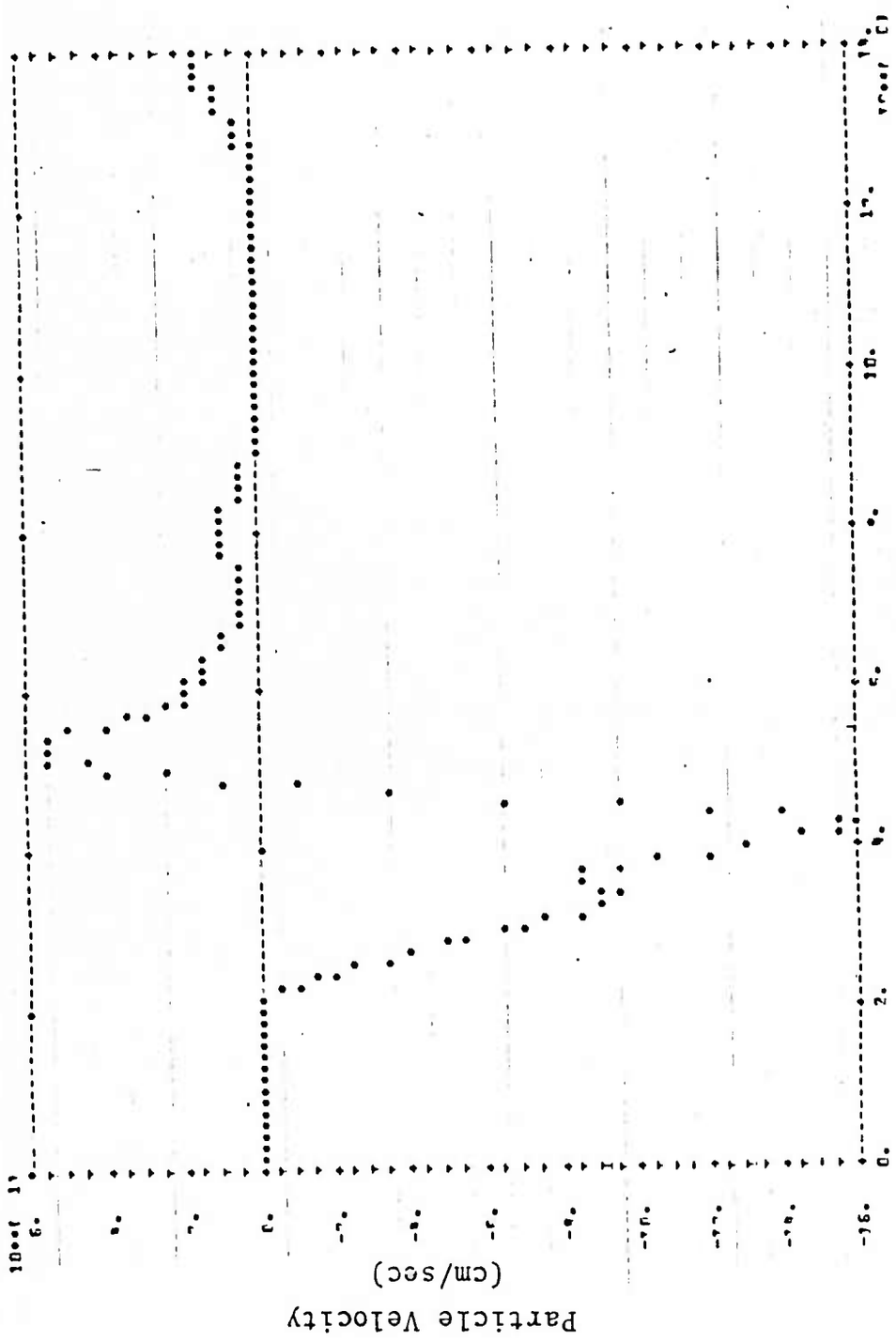

Fig. 10--Horizontal component of particle velocity at x = 0, y = -7.67 km for Calculation T-45.

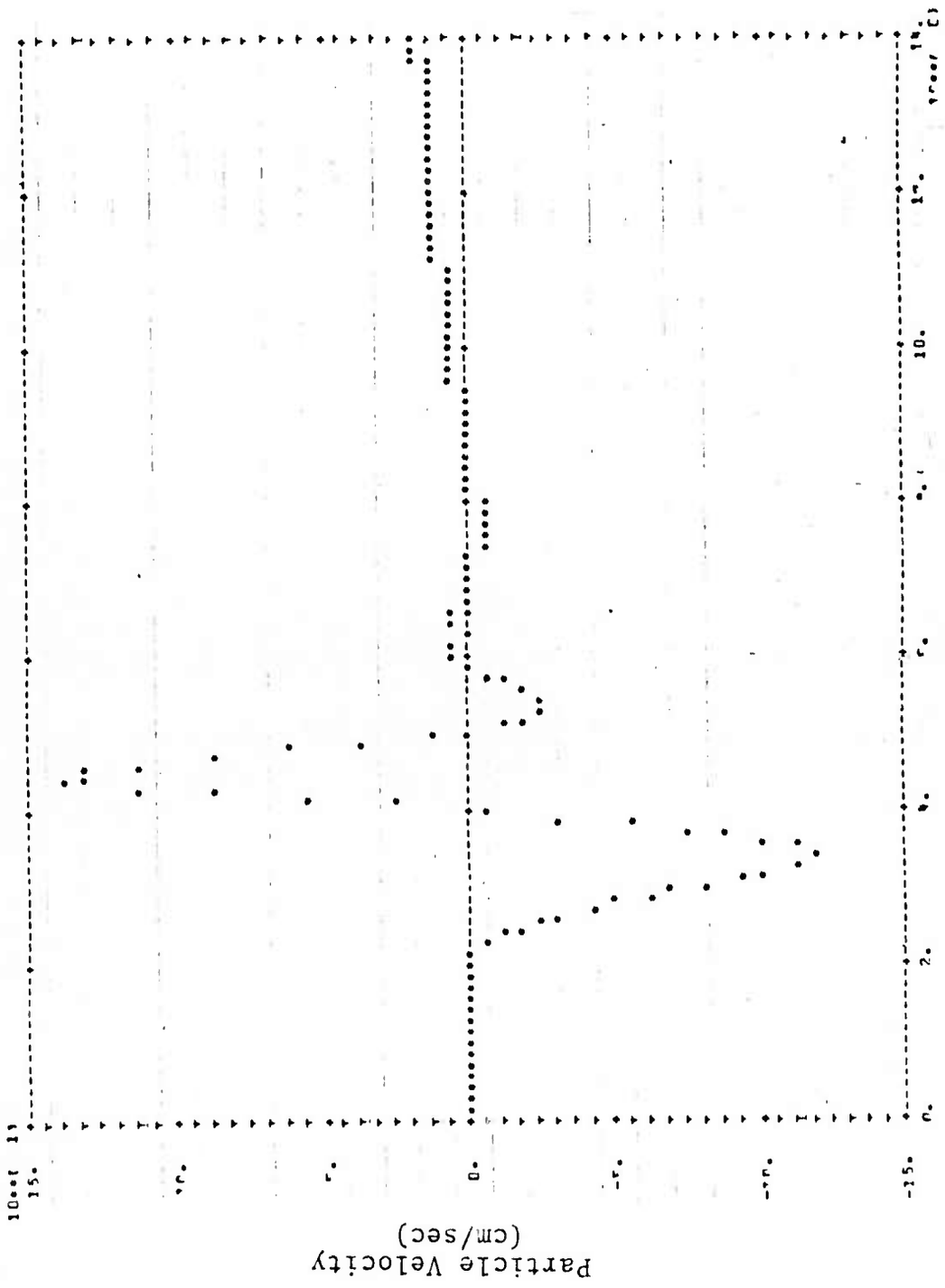

Fig. 11--Vertical component of particle velocity at x = 0, y = -7.67 km for Calculation T-45.

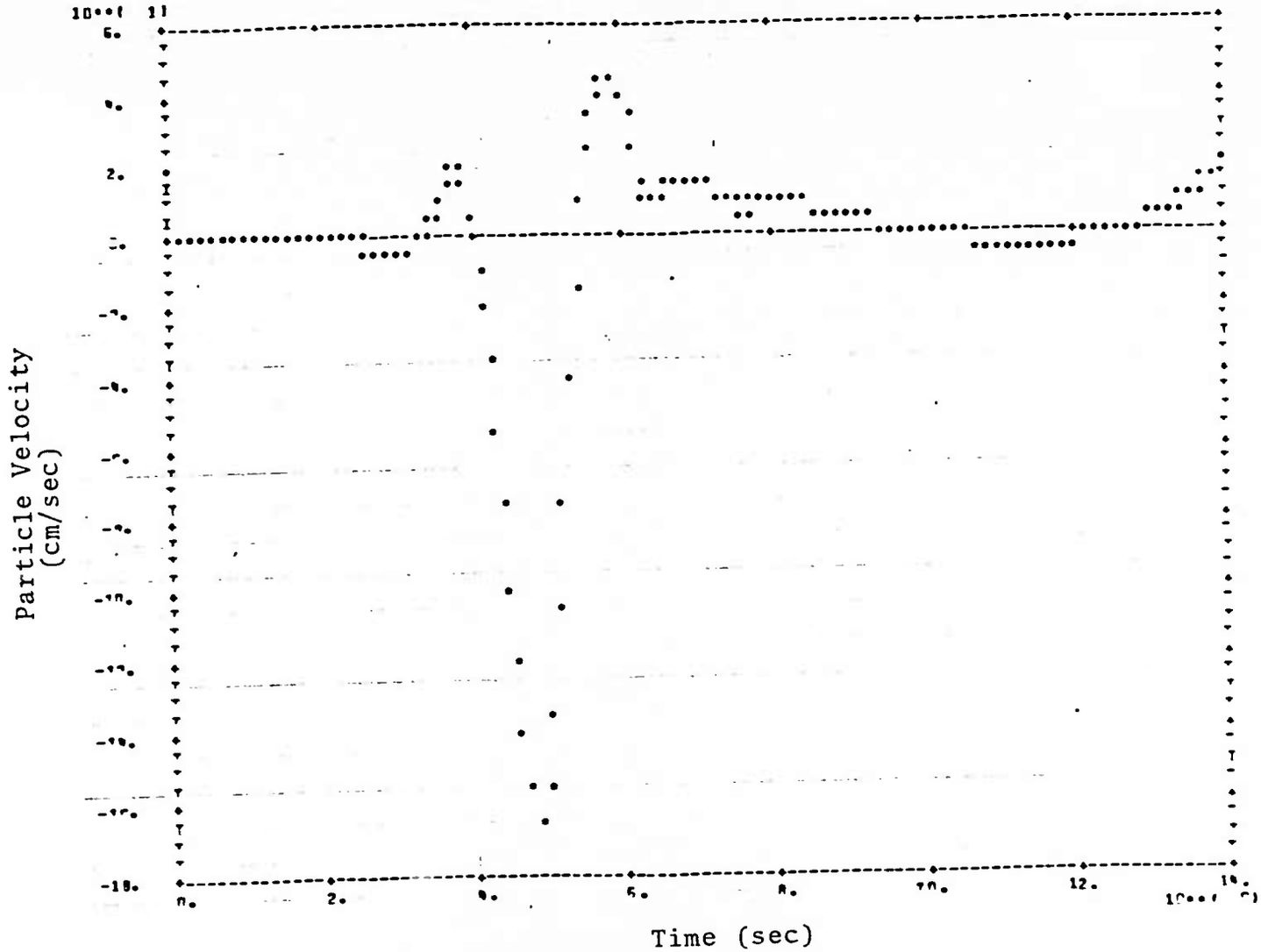

Fig. 12--Horizontal component of particle velocity at x = 0, y = -9.67 km for Calculation T-45.

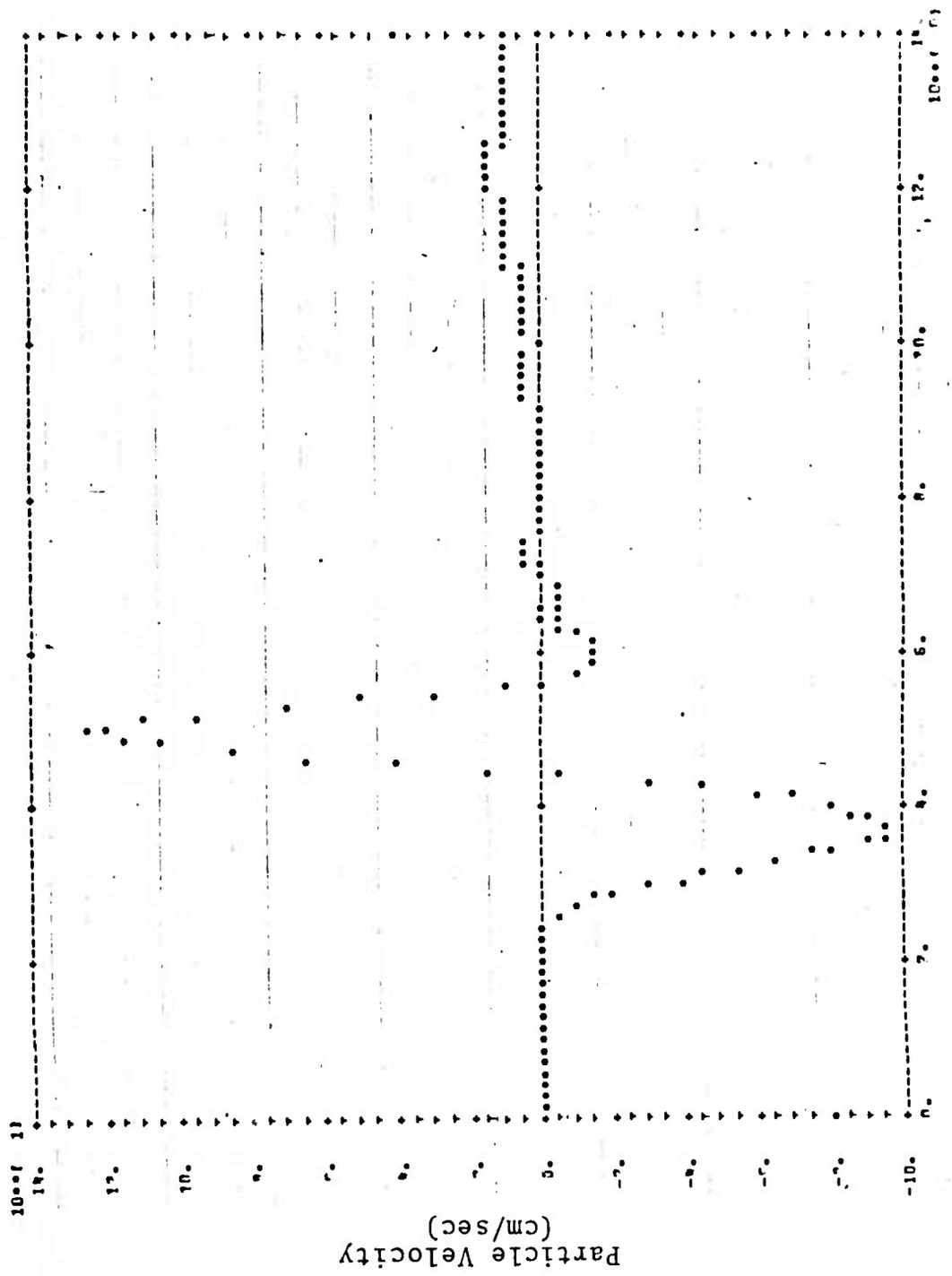

Fig. 13--Vertical component of particle velocity at x = 0, y = -9.67 km for Calculation T-45.

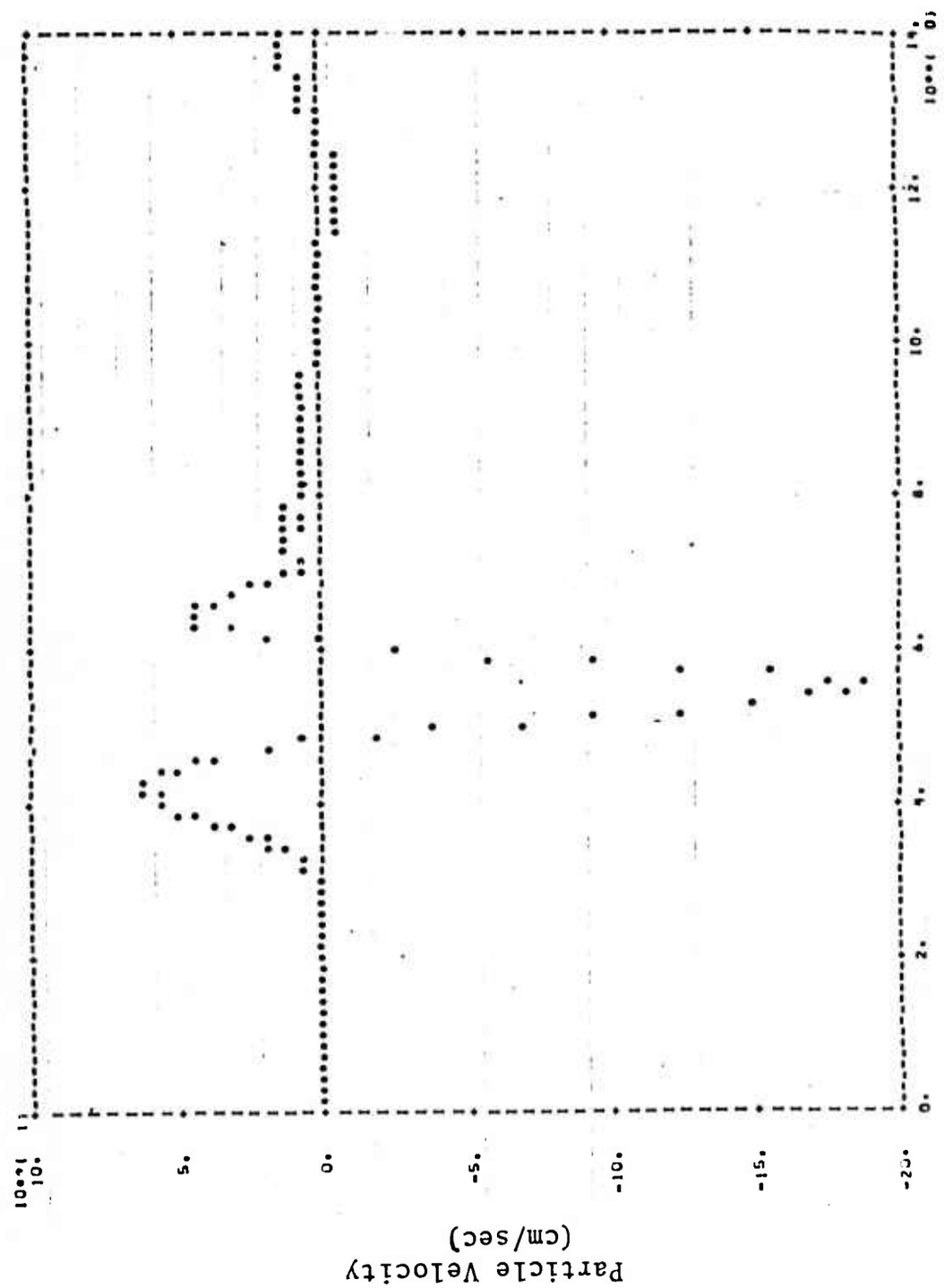

Fig. 14--Horizontal component of particle velocity at x = 0, y = -11.67 km for Calculation T-45.

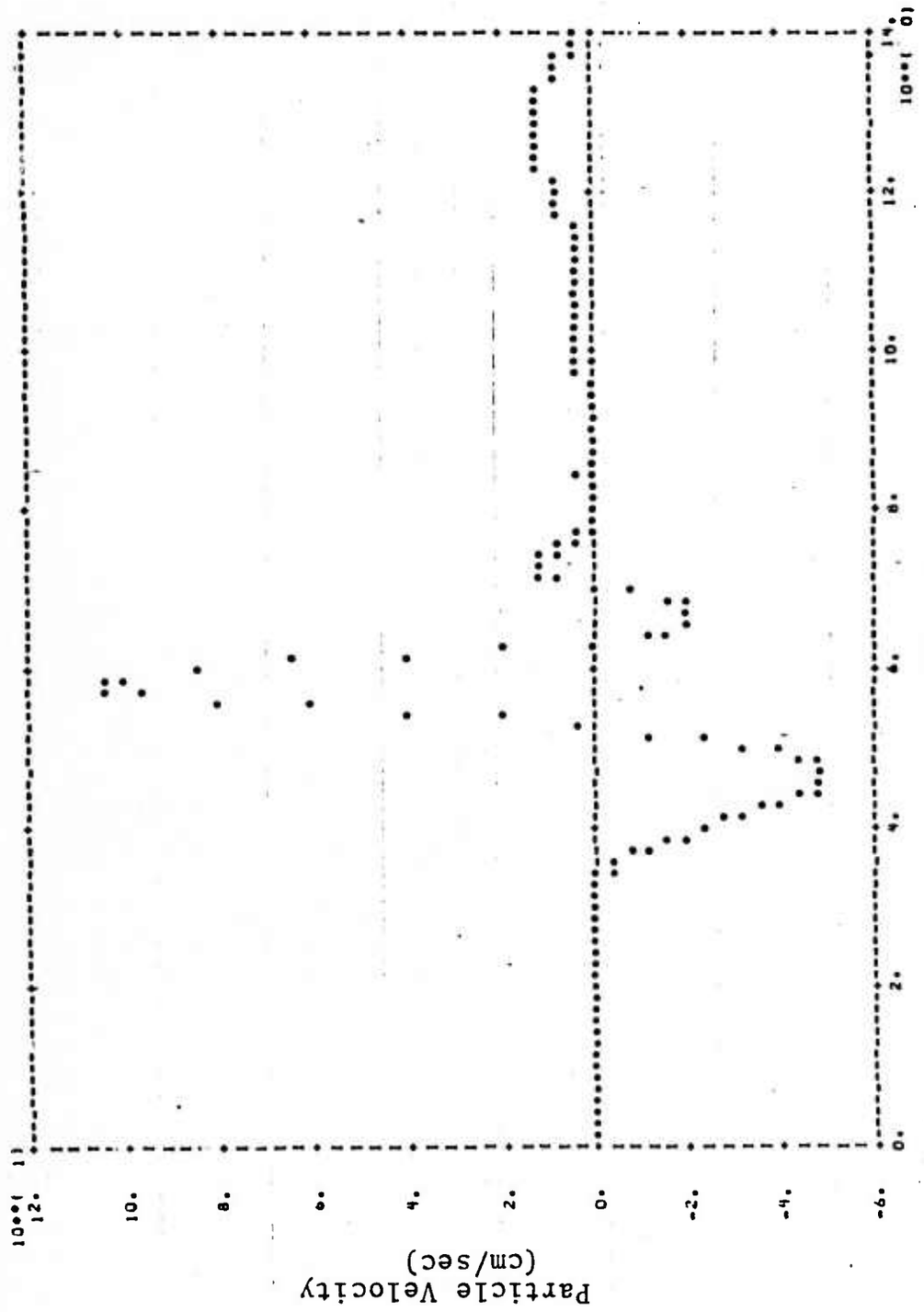

Fig. 15--Vertical component of particle velocity at x = 0, y = -11.67 km for Calculation T-45.

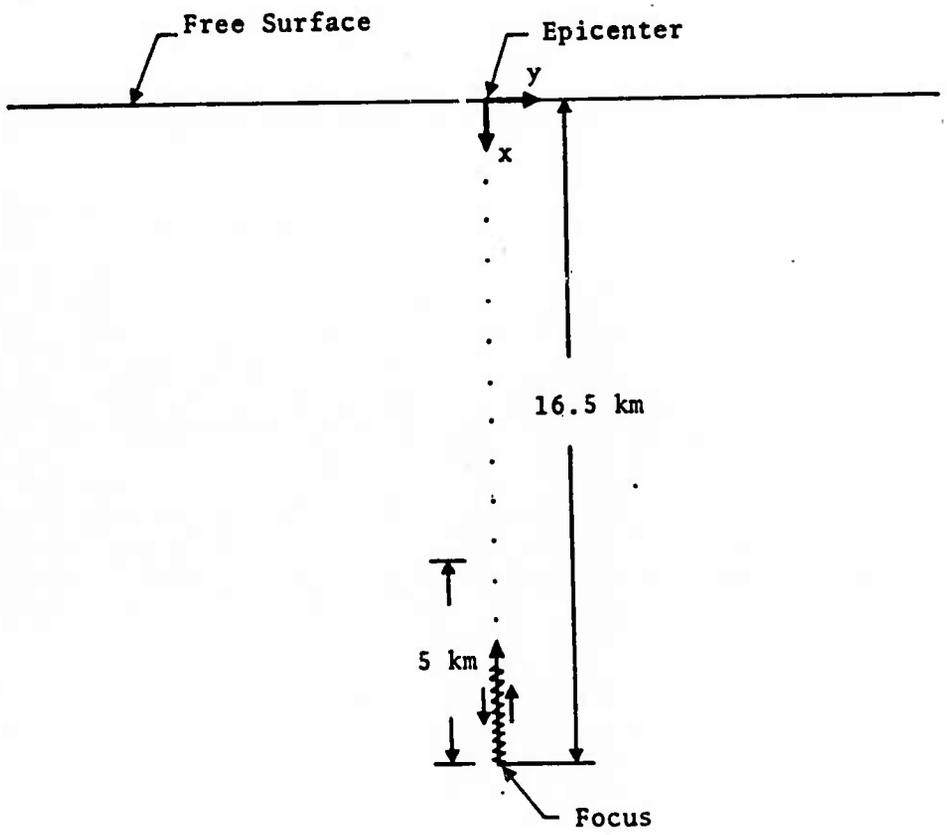

Fig. 16--Schematic of Calculation T-90. The focal depth was 16.5 km and the rupture length was 5 km. The stations monitored were at the free surface and to the left of the epicenter.

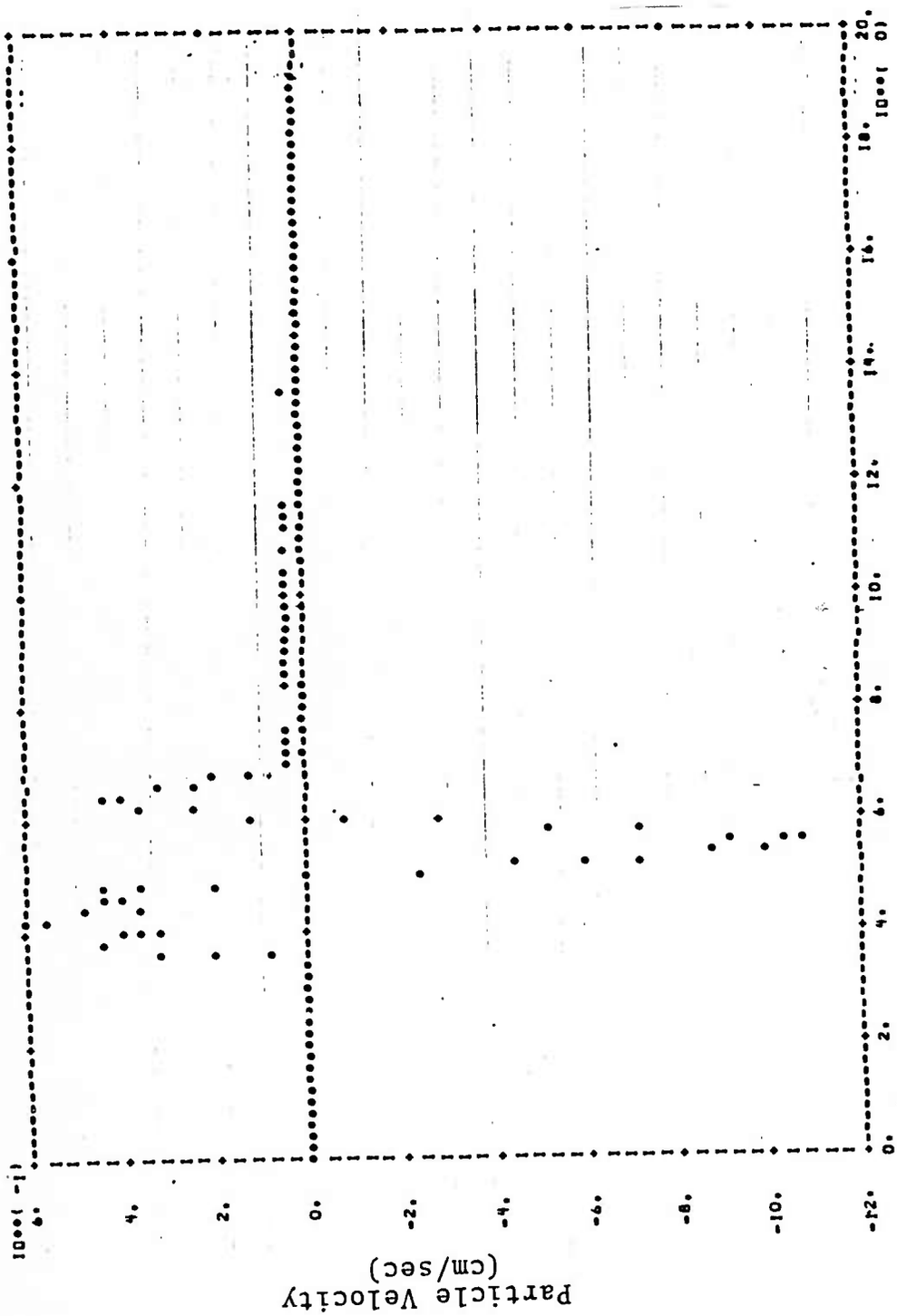

Fig. 17--Horizontal component of particle velocity at x = 0, y = 0 for Calculation T-90.

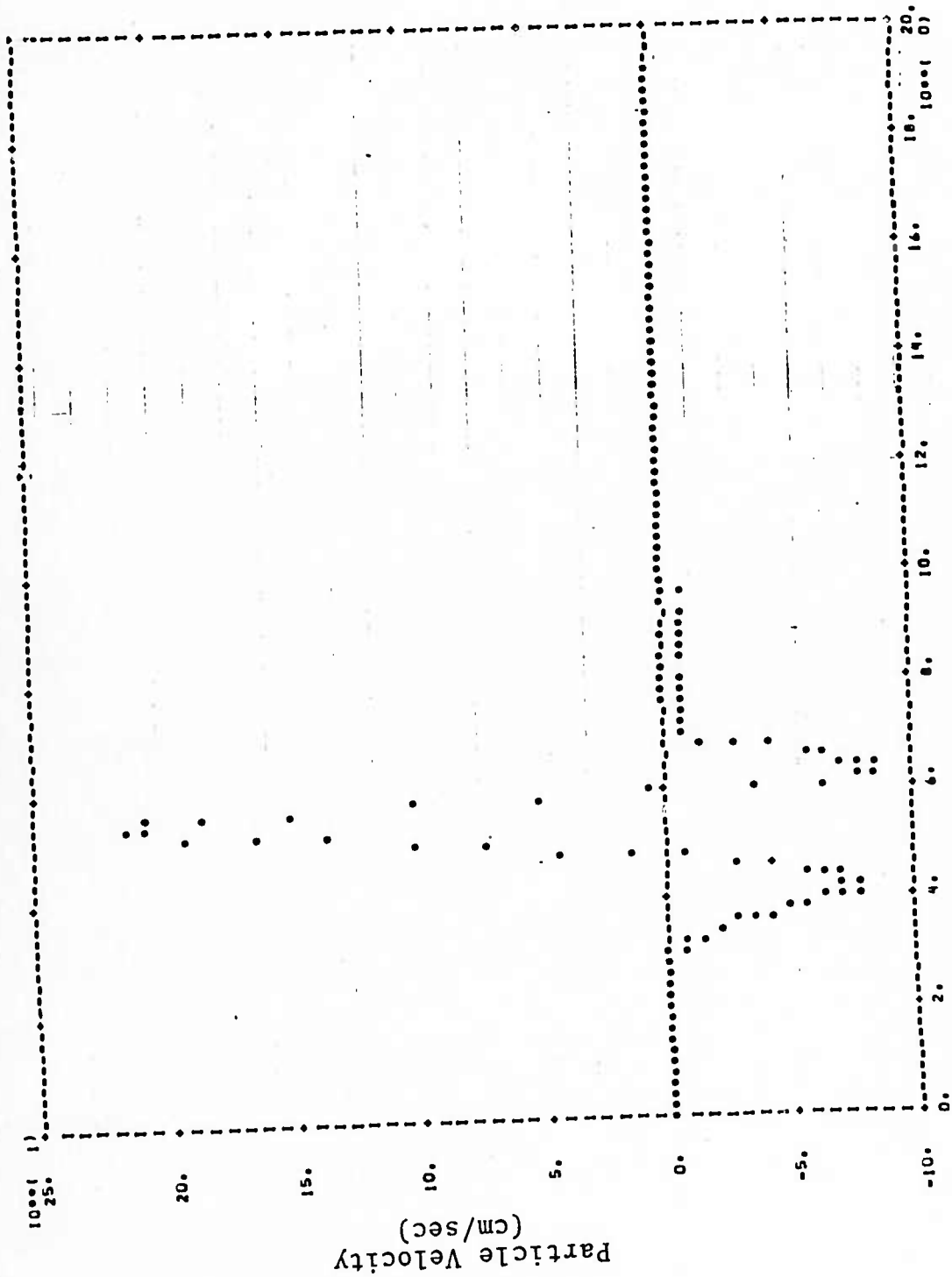

Fig. 18--Vertical component of particle velocity at x = 0, y = 0 for Calculation T-90.

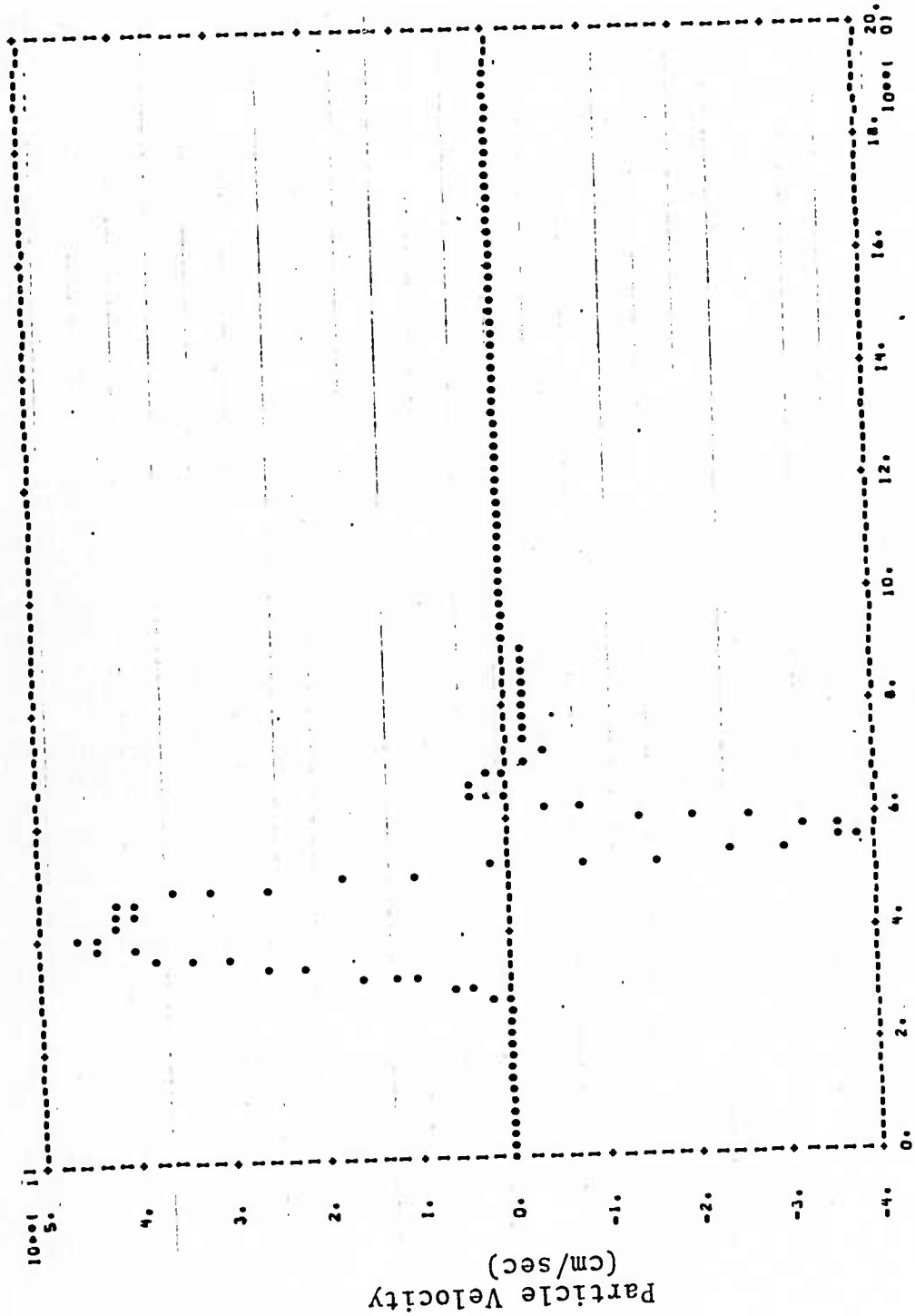

Fig. 19--Horizontal component of particle velocity at x = 0, y = -2 km for Calculation T-90.

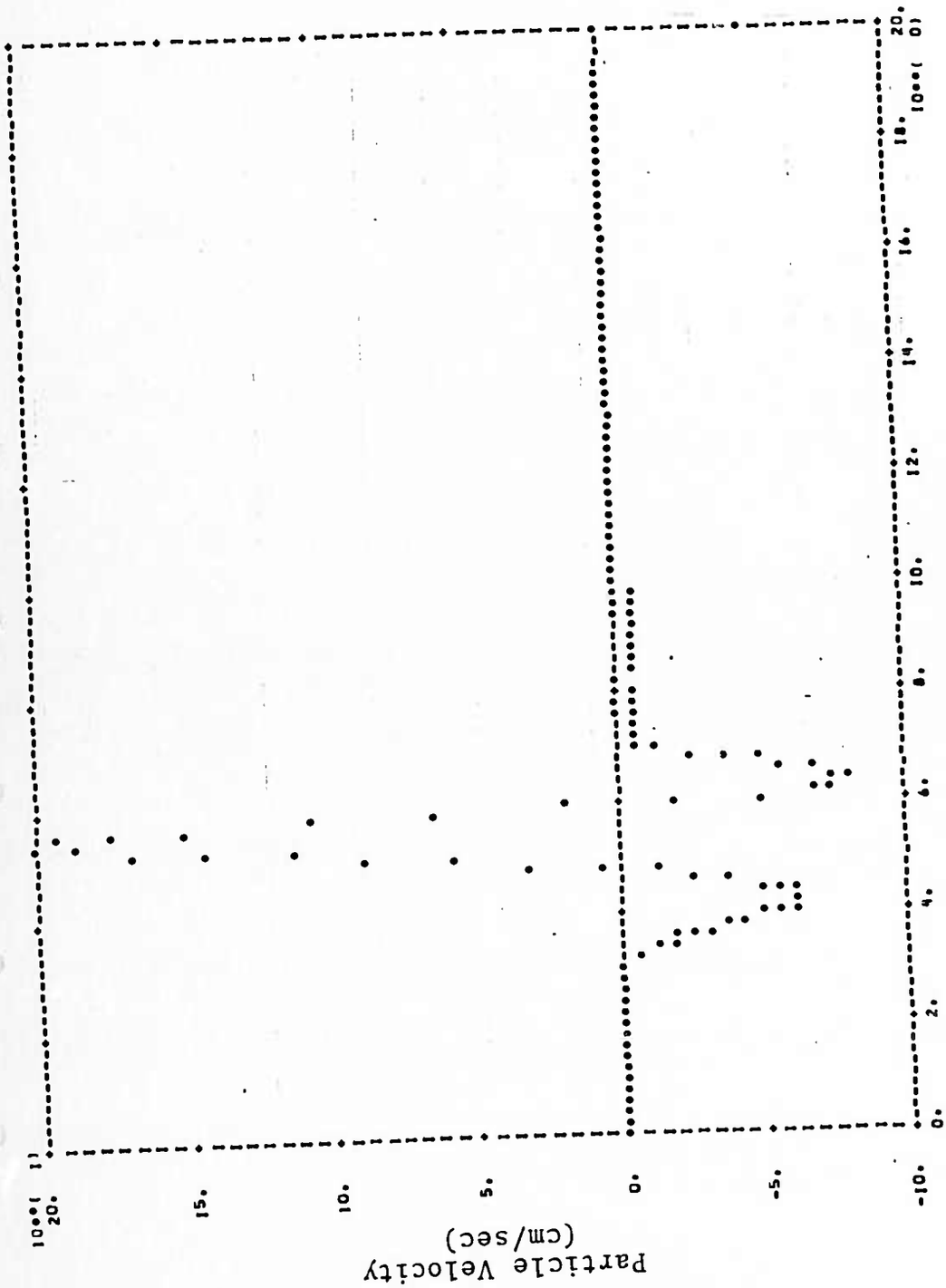

Fig. 20--Vertical component of particle velocity at x = 0, y = -2 km for Calculation T-90.

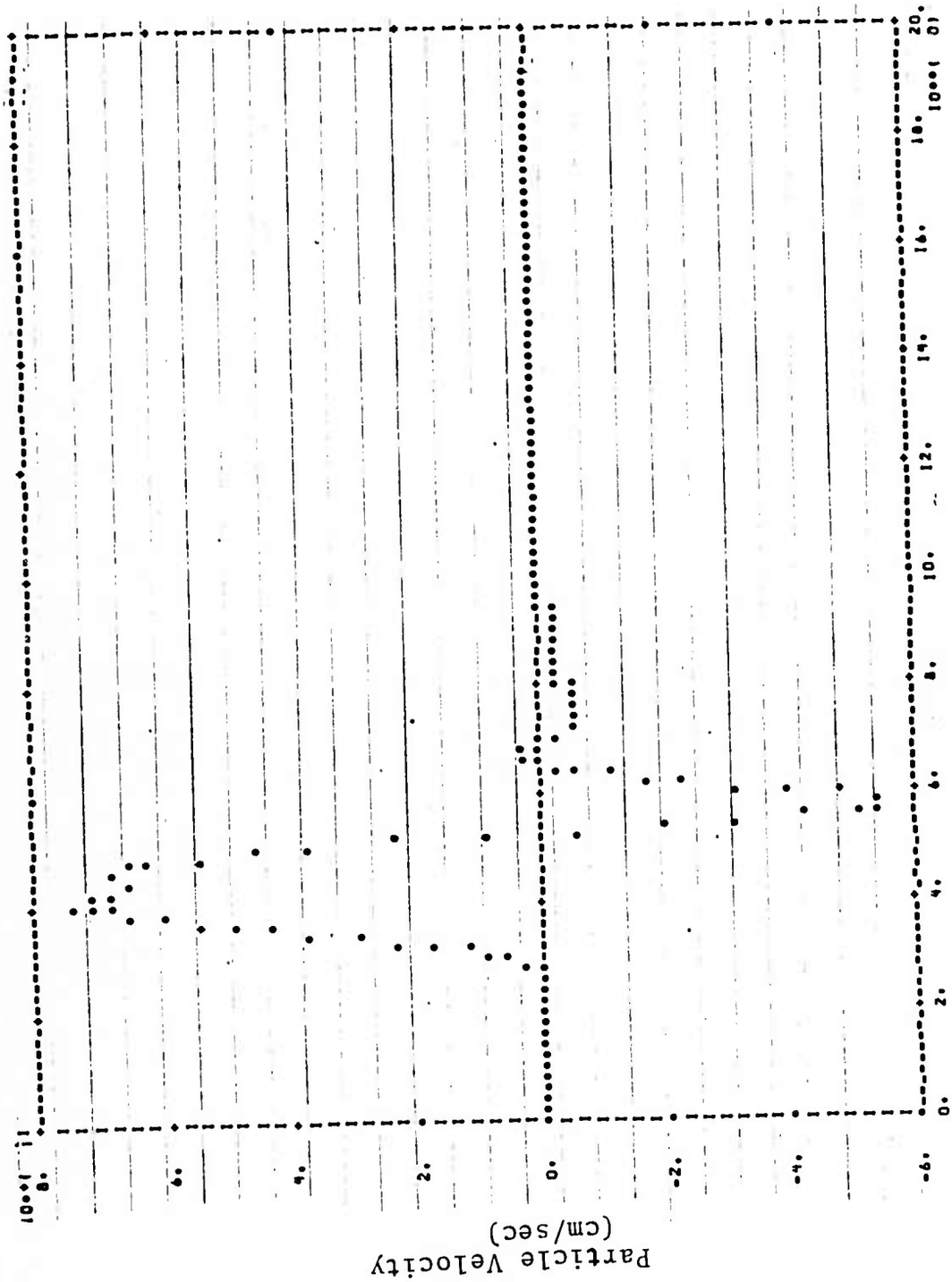

Fig. 21--Horizontal component of particle velocity at x = 0, y = -4 km for Calculation T-45.

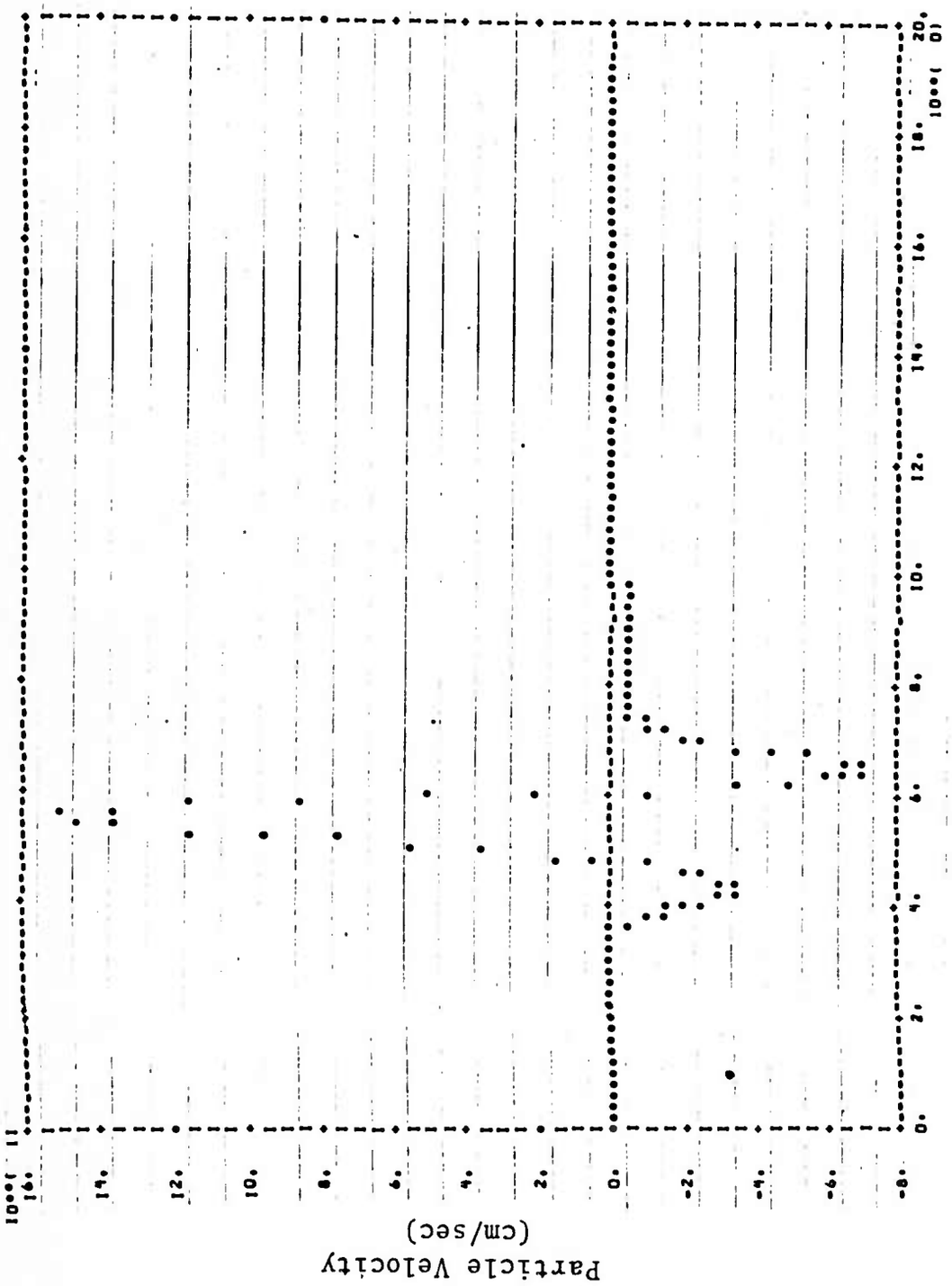

Fig. 22--Vertical component of particle velocity at x = 0, y = -4 km for Calculation T-45.

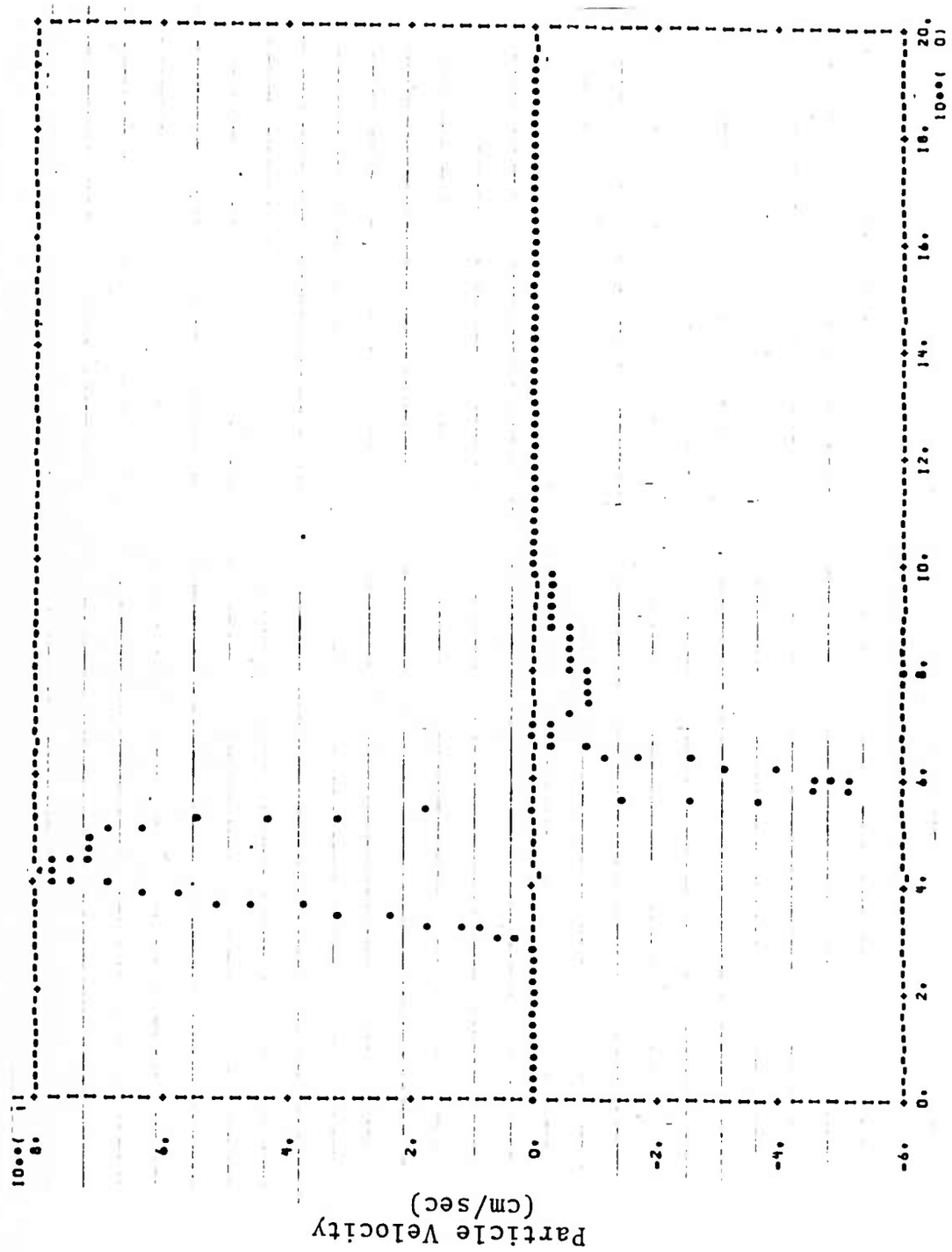

Fig. 23--Horizontal component of particle velocity at x = 0, y = -6 km for Calculation T-45.

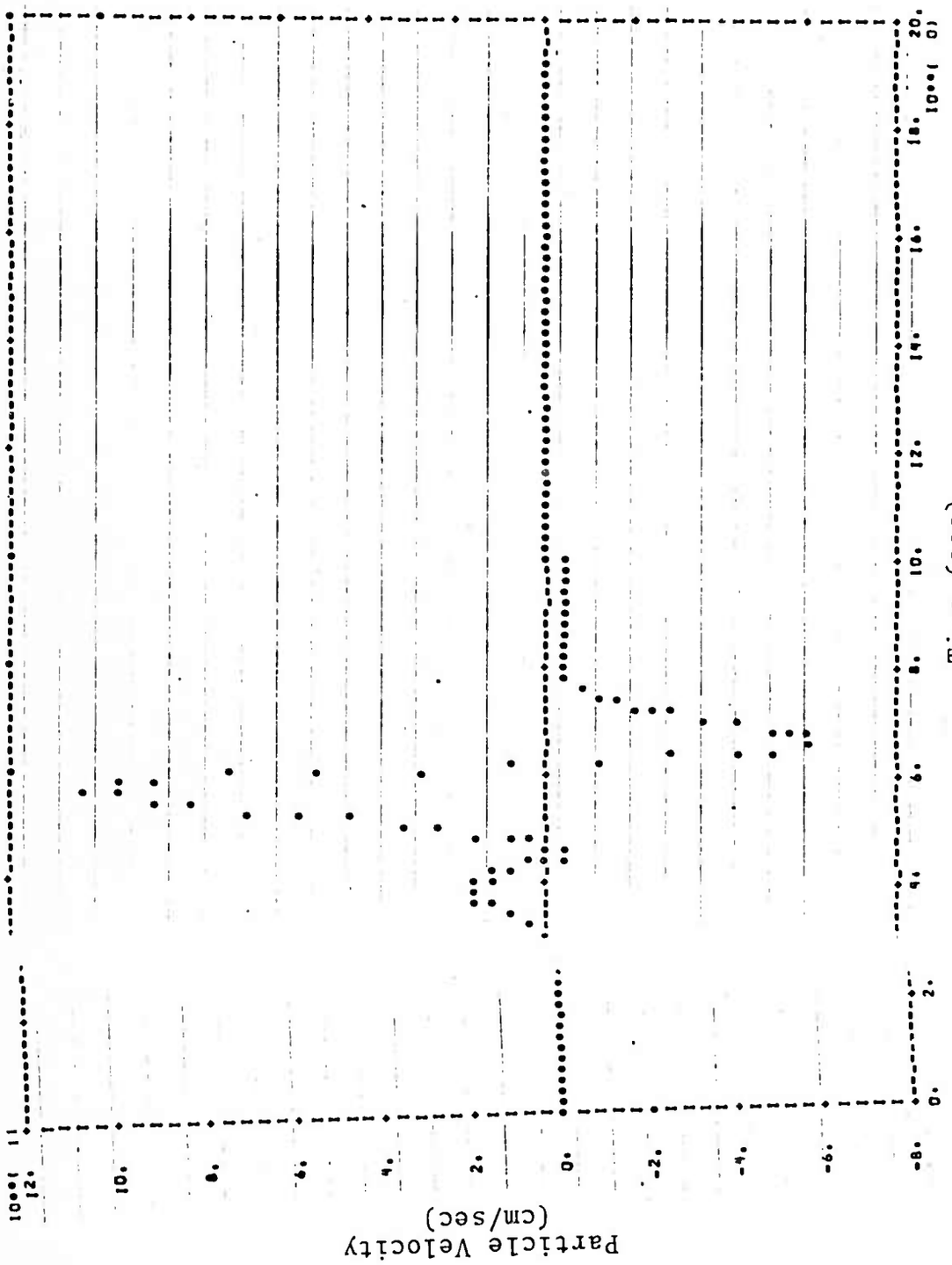

Fig. 24--Vertical component of particle velocity at x = 0, y = -6 km for calculation T-45.

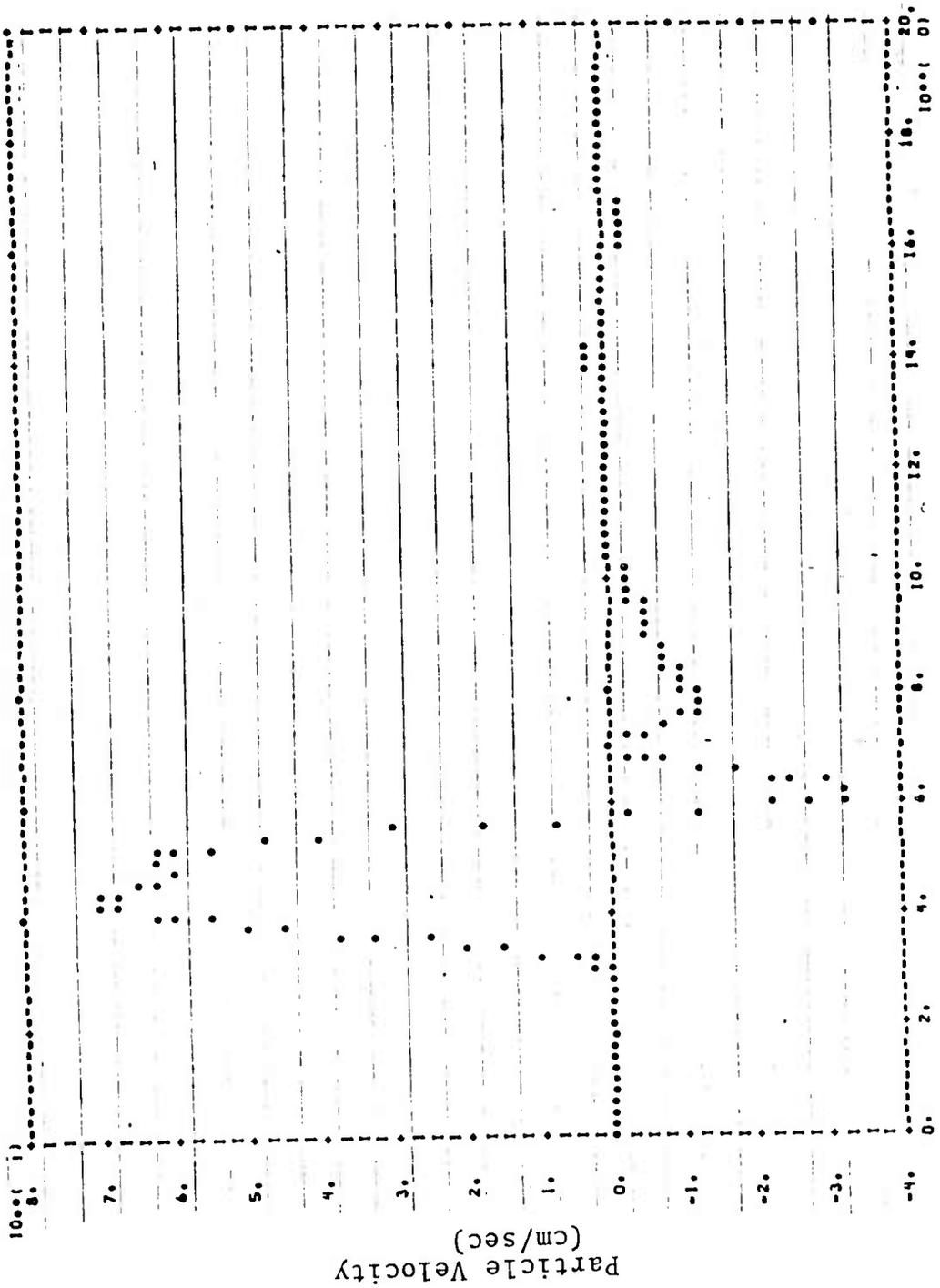

Fig. 25--Horizontal component of particle velocity at x = 0, y = -8 km for Calculation T-45.

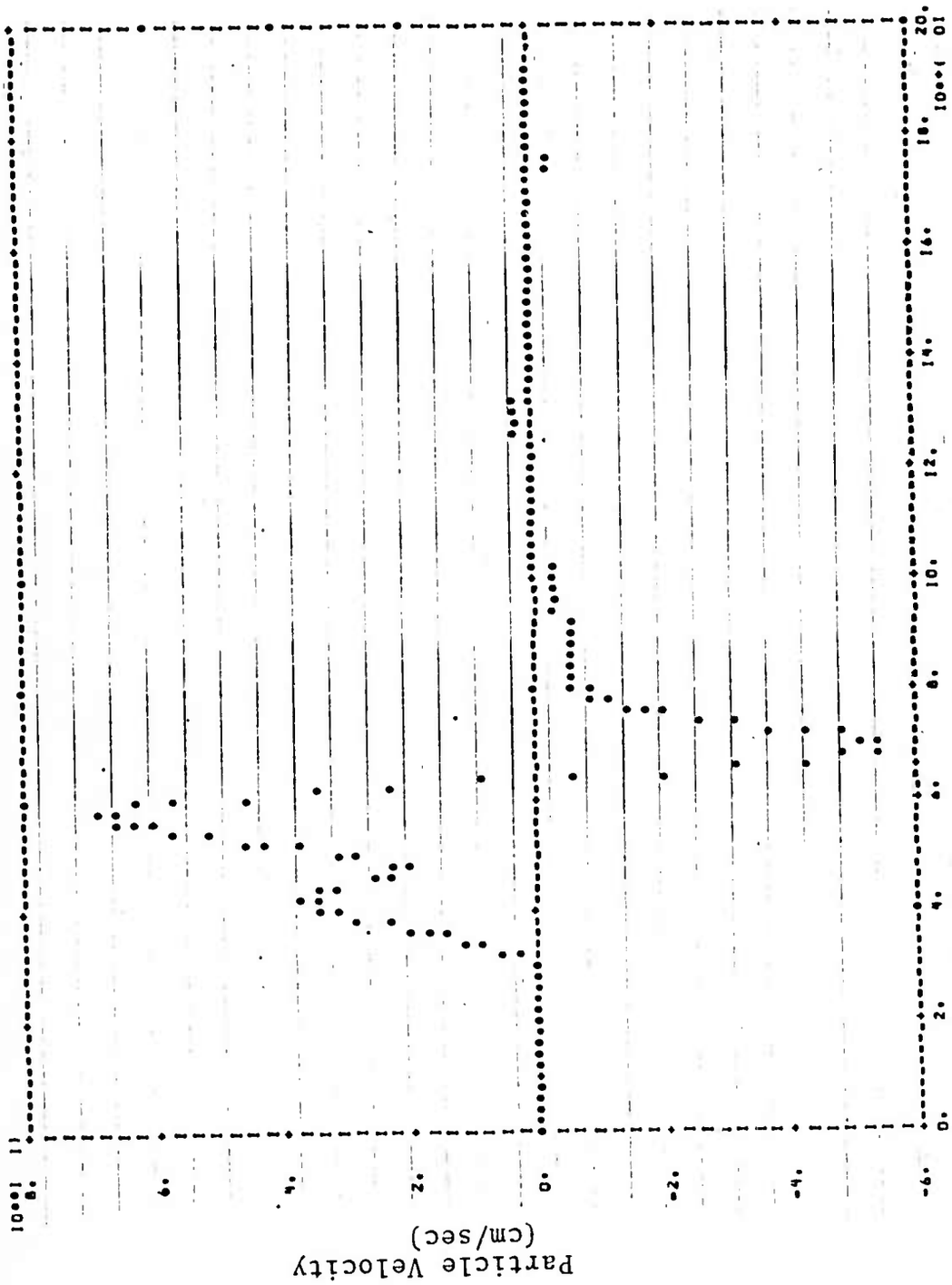

Fig. 26--Vertical component of particle velocity at x = 0, y = -8 km for Calculation T-45.

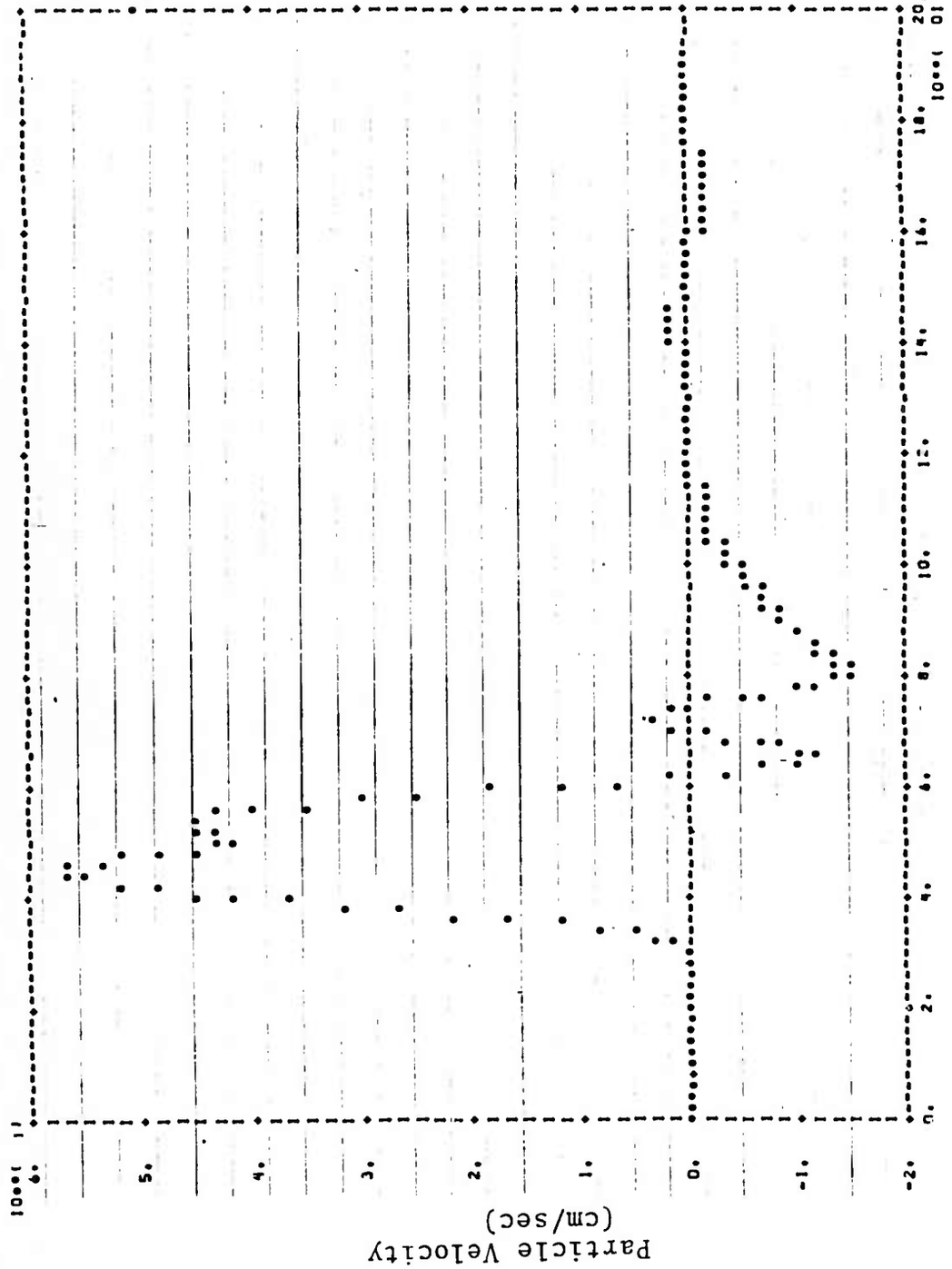

Fig. 27--Horizontal component of particle velocity at x = 0, y = -10 km for Calculation T-45.

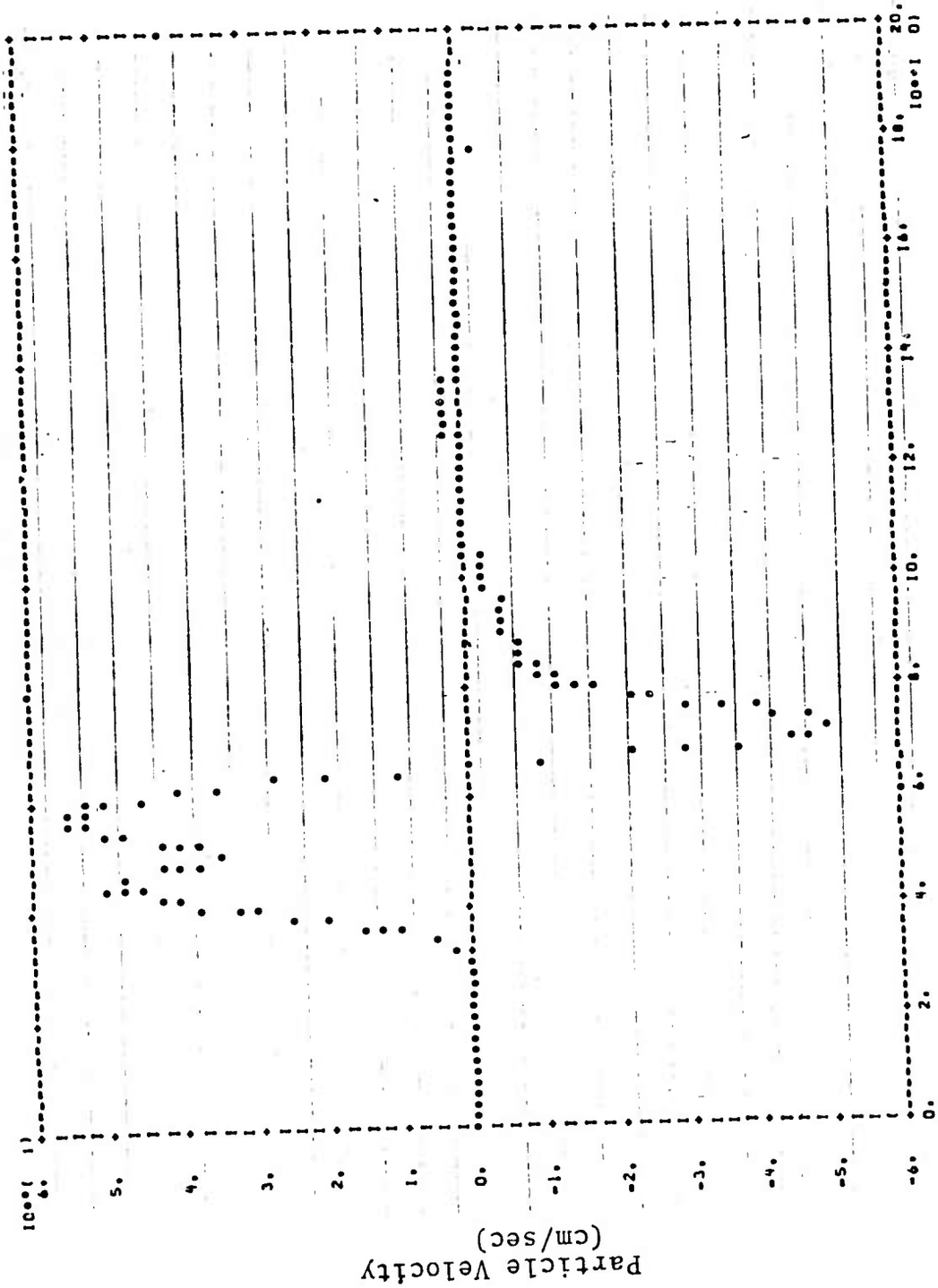

Fig. 28--Vertical component of particle velocity at x = 0, y = -10 km for Calculation T-45.

The maximum horizontal component of particle velocity is toward the epicenter, similar to the T-45 calculation. However, the maximum vertical ground motion is down for the T-90 calculation.

Figures 29 and 30 give the horizontal and vertical components of particle velocity recorded at Pacoima Dam during the February 9, 1971 San Fernando earthquake. The maximum horizontal component of particle velocity is toward the epicenter while the maximum on the vertical component is in the up direction.

Estimates of the focal depth of the San Fernando earthquake range between 8-14 km with Pacoima Dam located 9-12 km due south of the epicenter (Allen, et al., 1971, Hanks, 1973). Figures 31 and 32 give the horizontal and vertical components of particle velocity 9.67 km from the epicenter for the 45° thrust fault (calculation T-45). Figures 33 and 34 are the ground motion components 10 km from the epicenter for the vertical thrust fault (Calculation T-90).

The character of the ground motion at Pacoima Dam is best matched by the T-45 calculation. Also the calculated ground motion shown in Figs. 31 through 34 indicate that it should be possible to obtain a detailed match of the first few seconds of the Pacoima Dam seismograms by increasing the dip of the fault plane to a value greater than 45°.

It is interesting to note that the fault plane solution for the San Fernando earthquake gives a dip of 52° for the fault (Whitcomb, et al., 1973) and a maximum static displacement of 5 meters across the fault near the hypocenter. (Jangels and Frazier, 1973). Both results are consistent

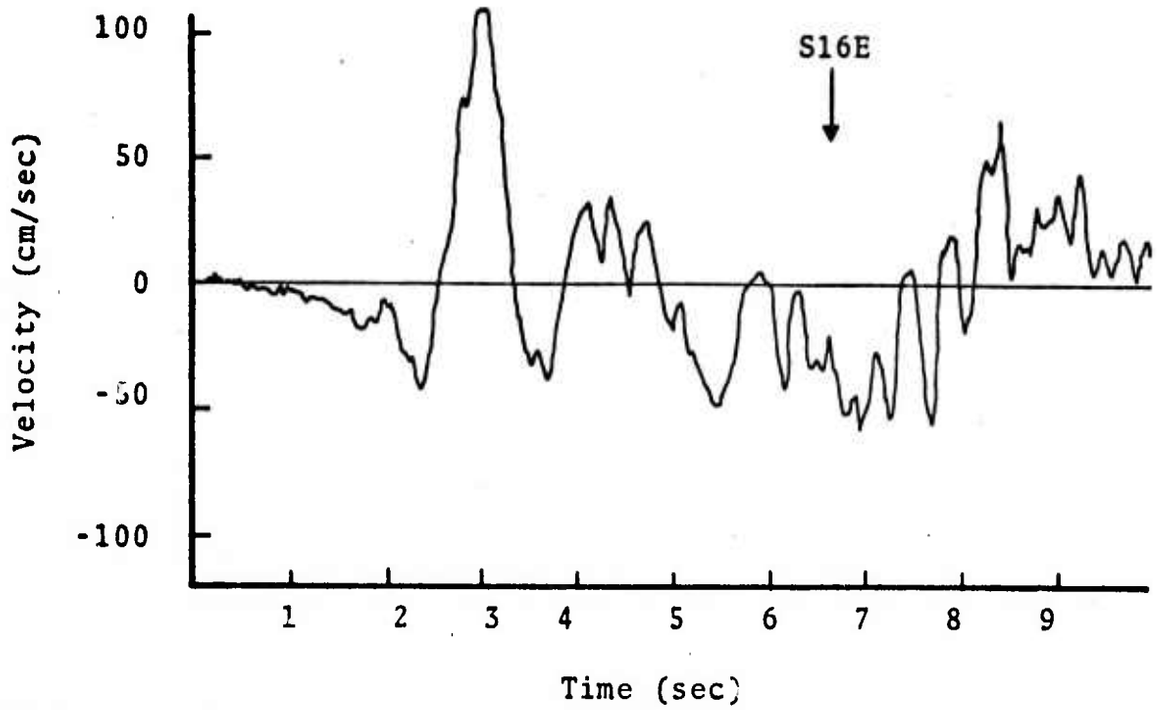

Fig. 29--Horizontal component of particle velocity at Pacoima Dam from the San Fernando Earthquake. Motion in the positive direction corresponds to ground velocity toward the epicenter.

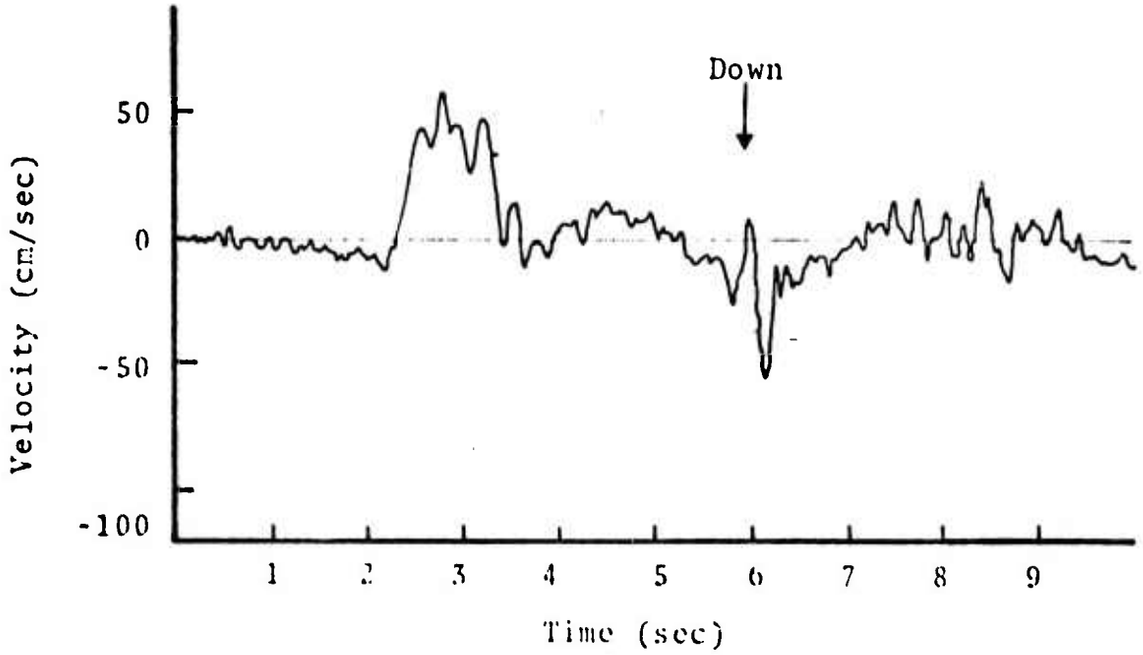

Fig. 30--Vertical component of particle velocity at Pacoima Dam from the San Fernando earthquake. Motion in the positive direction corresponds to ground velocity up.

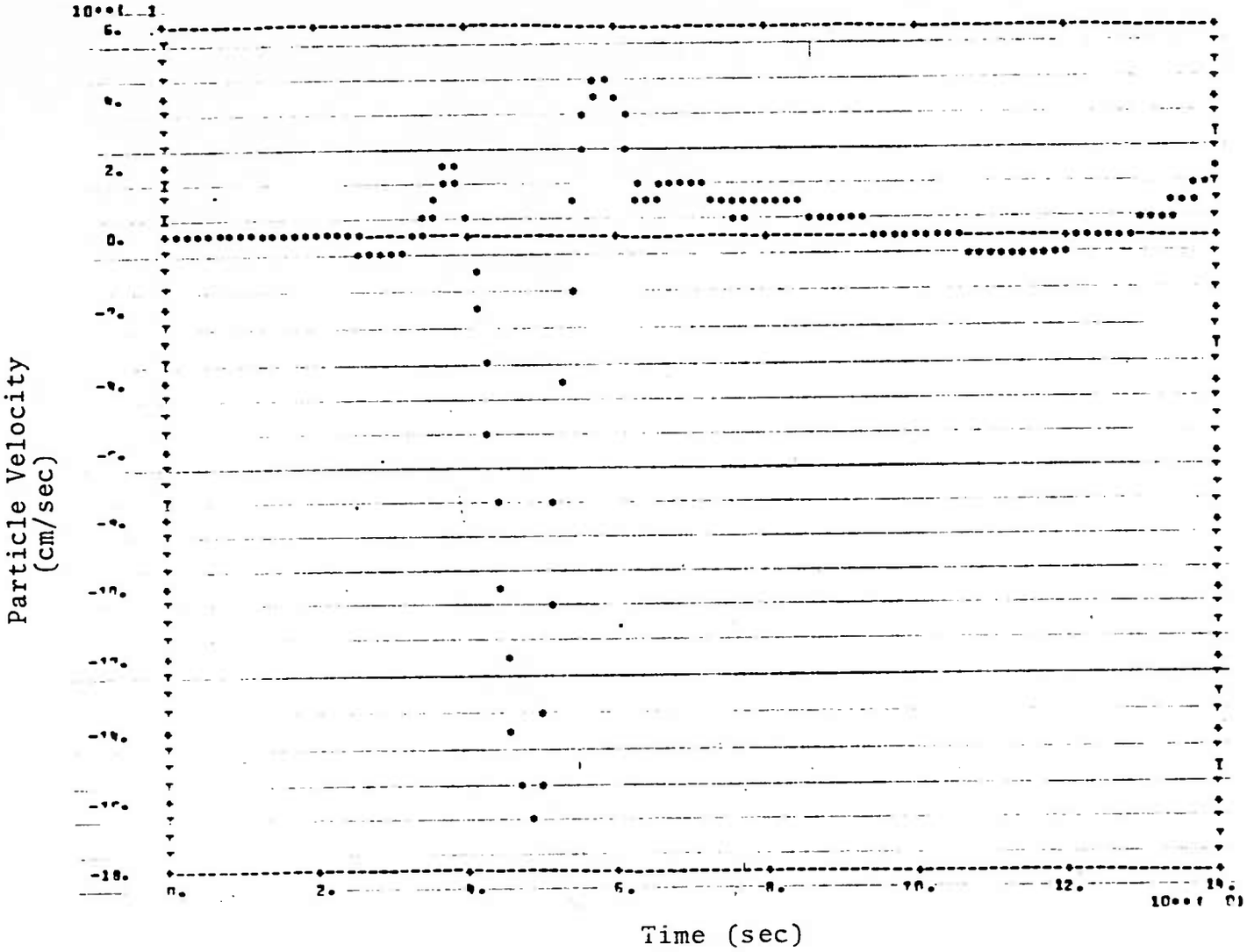

Fig. 31--Horizontal component of particle velocity 9.67 km from the epicenter from Calculation T-45. Positive direction is velocity toward the epicenter.

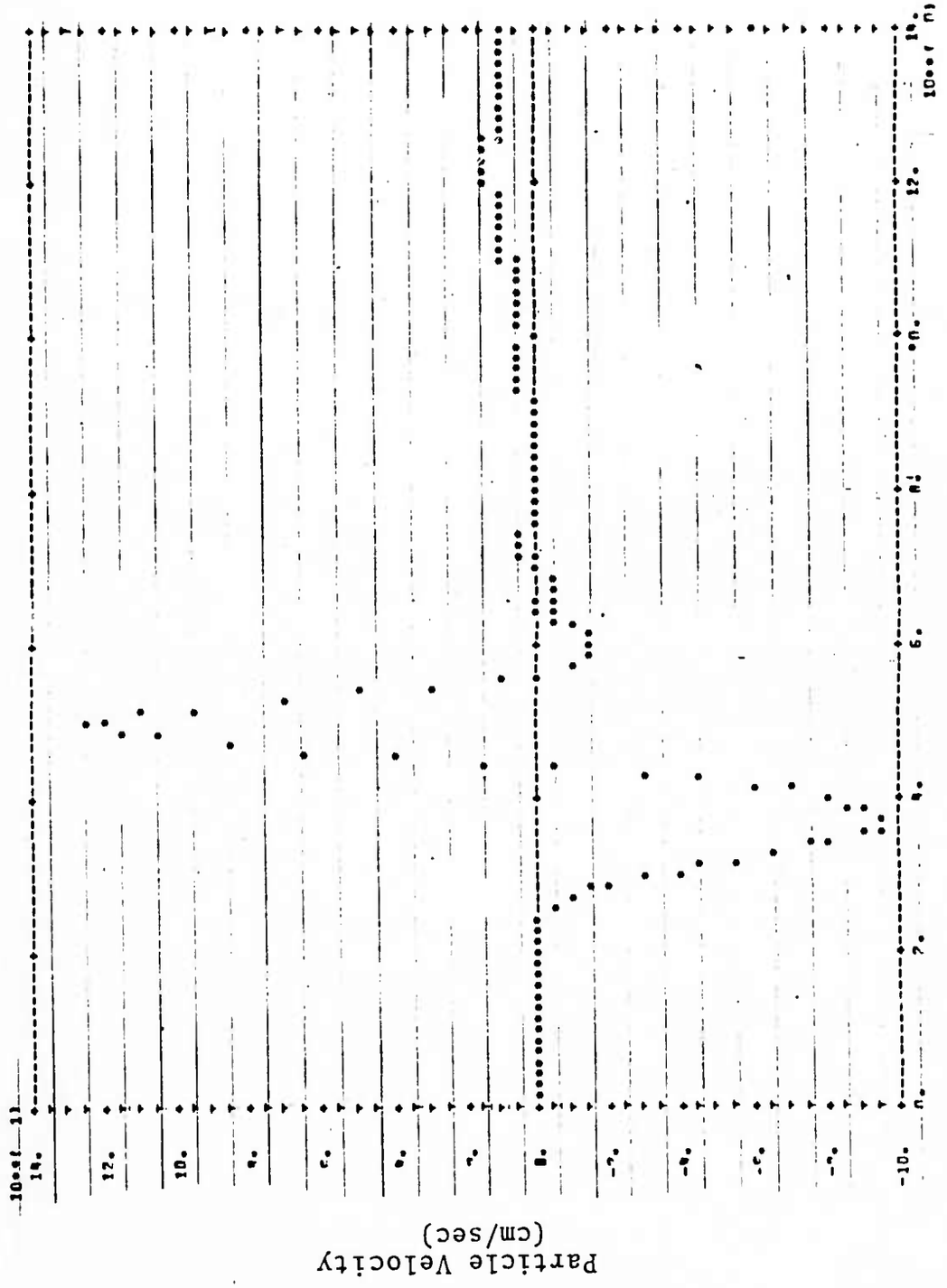

Fig. 32--Vertical component of particle velocity 9.67 km from the epicenter from Calculation T-45. Positive direction corresponds to ground velocity down.

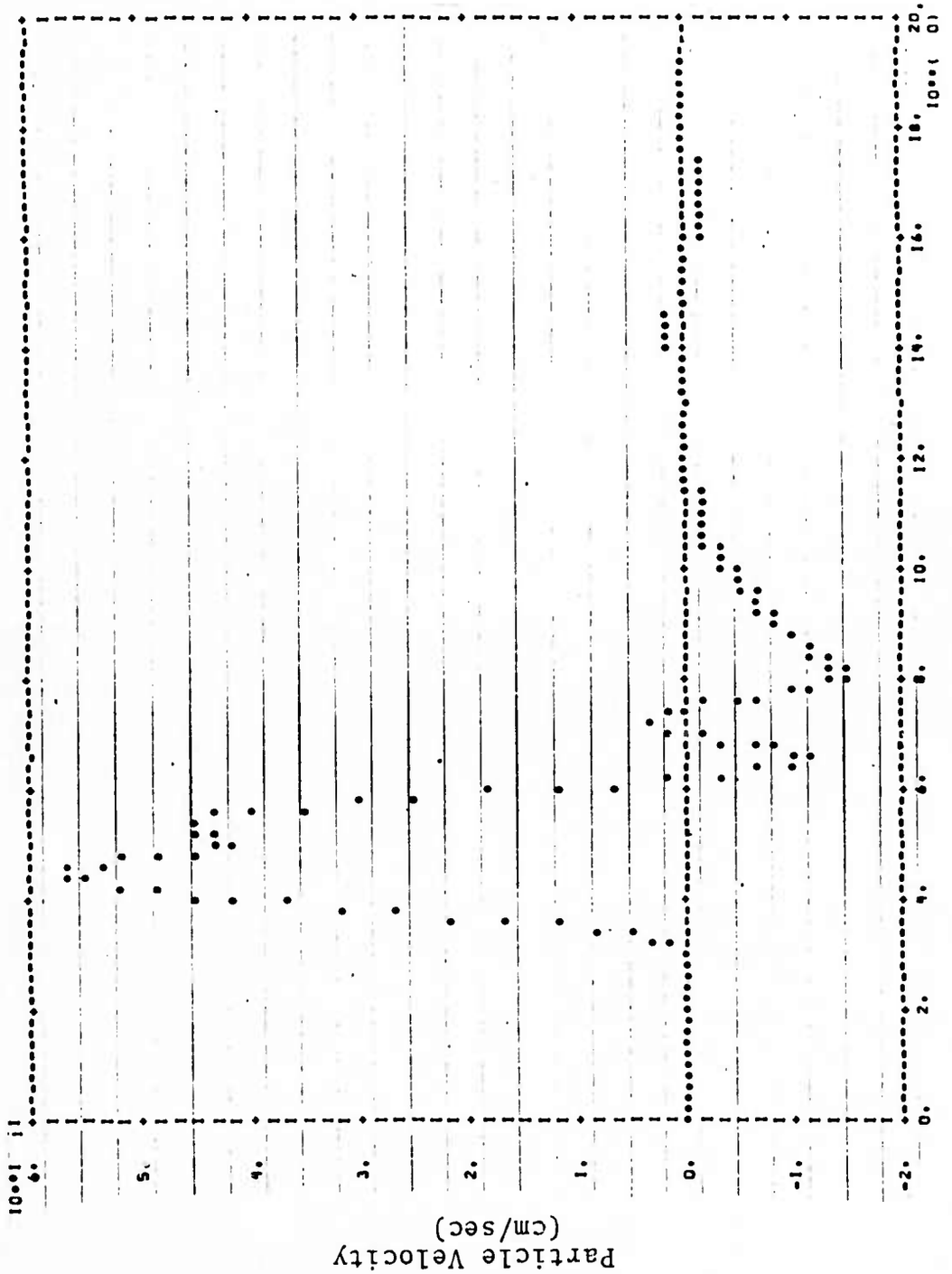

Fig. 33--Horizontal component of particle velocity 10 km from the epicenter from Calculation T-90. Positive direction is ground velocity toward the epicenter.

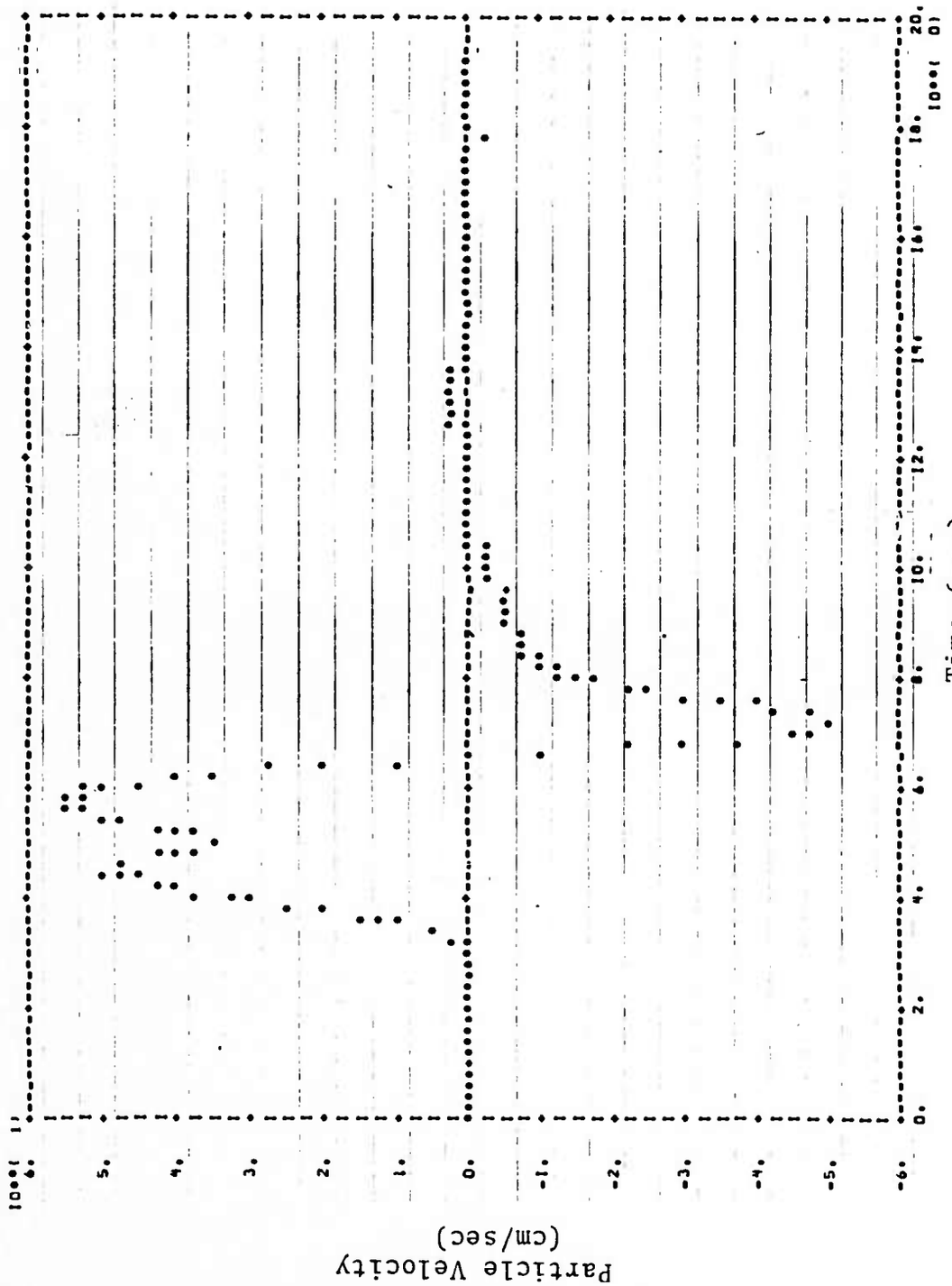

Fig. 34--Vertical component of particle velocity 10 km from the epicenter from Calculation T-90. Positive direction is ground velocity down.

with our calculations. Also, we agree with Hanks' (1973) conclusion that the San Fernando earthquake was initiated with massive but localized rupture in the hypocentral region. There seems little doubt that the rupture is capable of being simulated by the stick-slip process (Cherry, 1973) with the parameters in the model specified by data from laboratory tests on rock samples.

III. FREE FIELD DISPLACEMENT SPECTRA

The free field displacement spectra reported previously (Cherry, 1973)* were obtained at distances of the order of two fault dimensions from the center of the fault and were contaminated by near field effects. In an attempt to uncover the nature of the free field displacement spectrum we performed a calculation and monitored free field ground motion five fault dimensions away from the center of the fault.

Figure 35 is a schematic of the calculation. The fault length was 1 km. The dynamic stress drop was 0.25 kbar and the rupture velocity equaled 2.3 km/sec. The maximum relative displacement across the fault was 0.247 m and occurred 0.35 km from the focus.

Figure 36 is the spectrum of the y component of displacement at $R = 5$ km, $\theta = 180°$. The high frequency portion of the spectrum decays as f^{-3}. The corner frequency is approximately 1.9 Hz ($10^{+.28}$) and the spectrum is flat in the interval 0.2 Hz < f < 1 Hz. The relation established by Cherry (1973) between corner frequency (f_c), fault length (L)

---

*In that report the FFT of particle velocity was divided by the frequency in Hz to obtain the displacement spectrum. This division introduces a factor of 2π in the spectrum. Therefore if $u(t)$ is ground displacement, then the displacement spectrum $\hat{u}$ is given by

$$\hat{u} = 2\pi \int_{-\infty}^{\infty} u(t) e^{-i\omega t} \, dt$$

This definition of the displacement spectrum is maintained in this report.

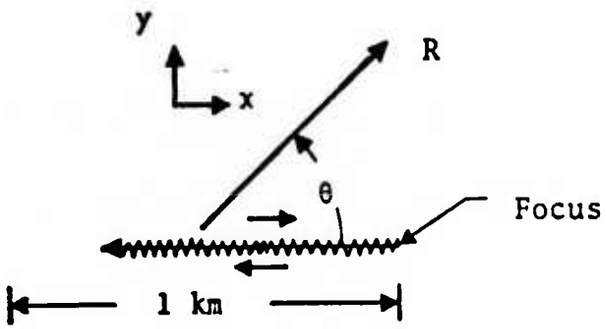

Fig. 35--Schematic of "far field" calculation. The fault length was 1 km and the stations monitored were 5 km from the center of the fault.

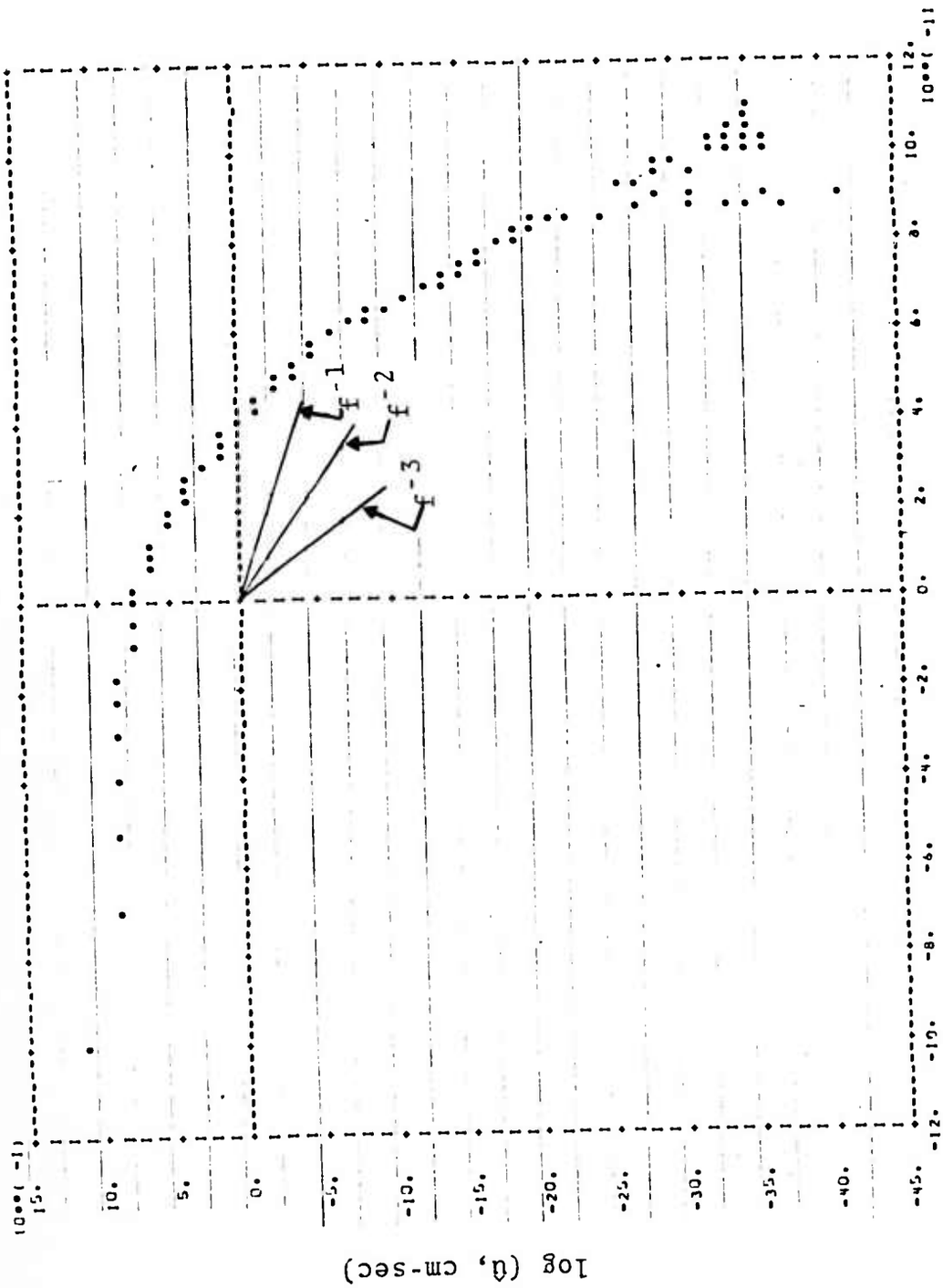

Fig. 36--Displacement spectrum at R = 5 km, θ = 180° from the y component of displacement. The corner frequency was chosen at the intersection of the f^{-3} and f^{0} components of the spectrum, i.e., $f_c = 10^{.28} = 1.9$ Hz.

and rupture velocity (V_R) at this azimuth is

$$f_c = 0.16 + 0.7 \left(\frac{V_R}{L}\right) .$$

This gives $f_c = 1.77$ Hz for $V_r = 2.3$ km/sec and $L = 1$ km.

Figure 37 is the displacement spectrum for the x component of displacement at $R = 5$ km, $\theta = 100°$. The spectrum is similar to that of Fig. 36 except the corner frequency has shifted to 0.9 Hz ($10^{-0.05}$) due to a Doppler effect from the finite rupture velocity. At this azimuth Cherry (1973) obtained the relation

$$f_c = 0.15 + 0.3 \left(\frac{V_R}{L}\right) .$$

This gives $f_c = 0.84$ Hz for $V_R = 2.3$ km/sec and $L = 1$ km.

Figure 38 is the spectrum at the epicenter for the vertical fault discussed in Section II (Calculation T-90) and shows the effect of the free surface in shaping the spectrum. Apparently spectral peaking in the epicentral region is caused by Rayleigh wave generation at the free surface, which provides a mechanism for reducing the static displacement from twice its free field value. Since the high frequency components of the incident wave are amplified by the free surface a peaked spectrum results.

Therefore, we should be careful in deducing the nature of the free field spectrum from near field, surface measurements until the effect of the free surface on the spectrum is understood. This is especially true for thrust and normal faults where the incident wave contains large P and SV components. The SH component of ground motion at Bear Valley should be heavily weighted when the spectral content of the source is deduced from field data.

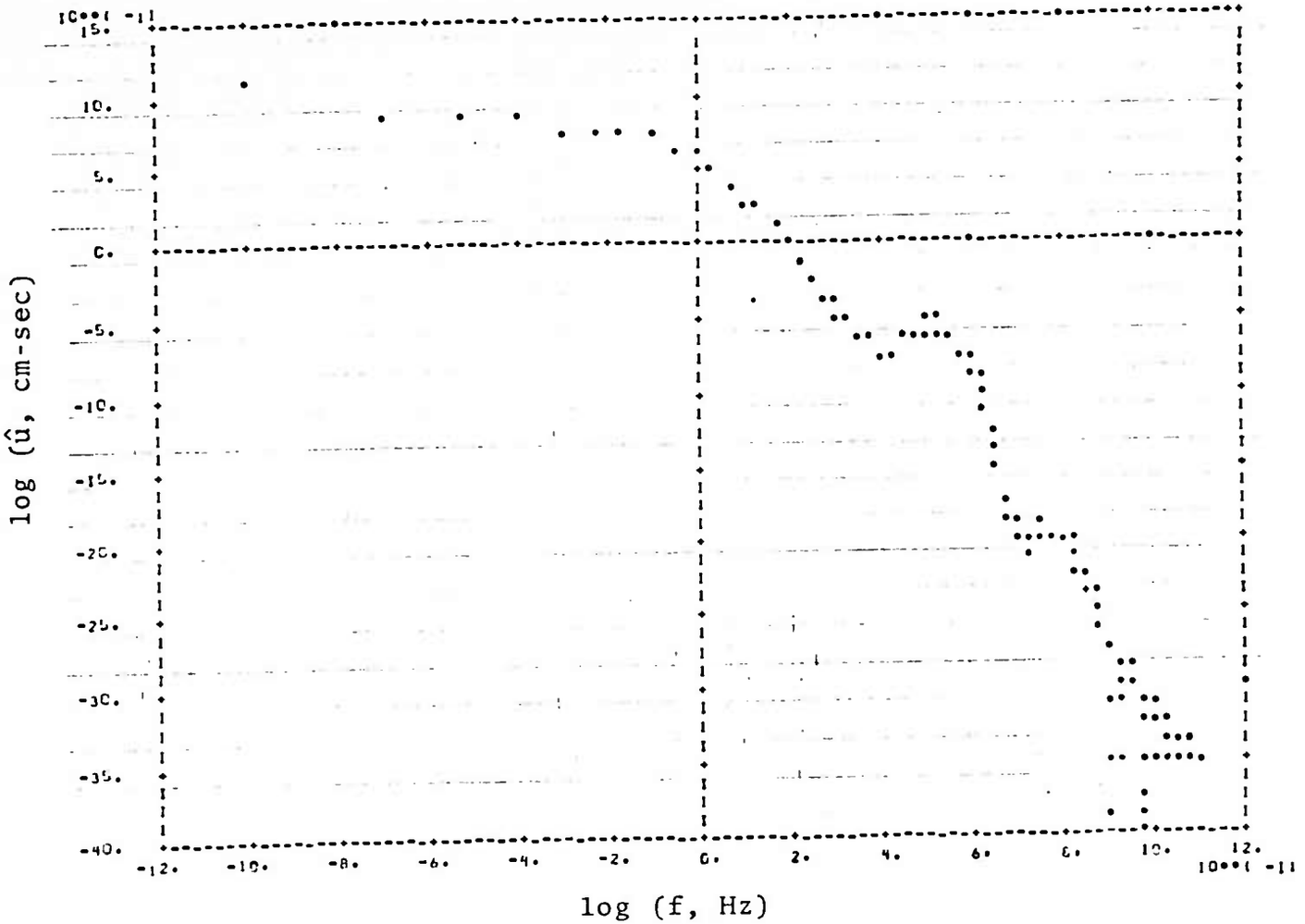

Fig. 37--Displacement spectrum at R = 5 km, θ = 100° for the x component of displacement. The corner frequency has shifted to 0.9 Hz at this azimuth.

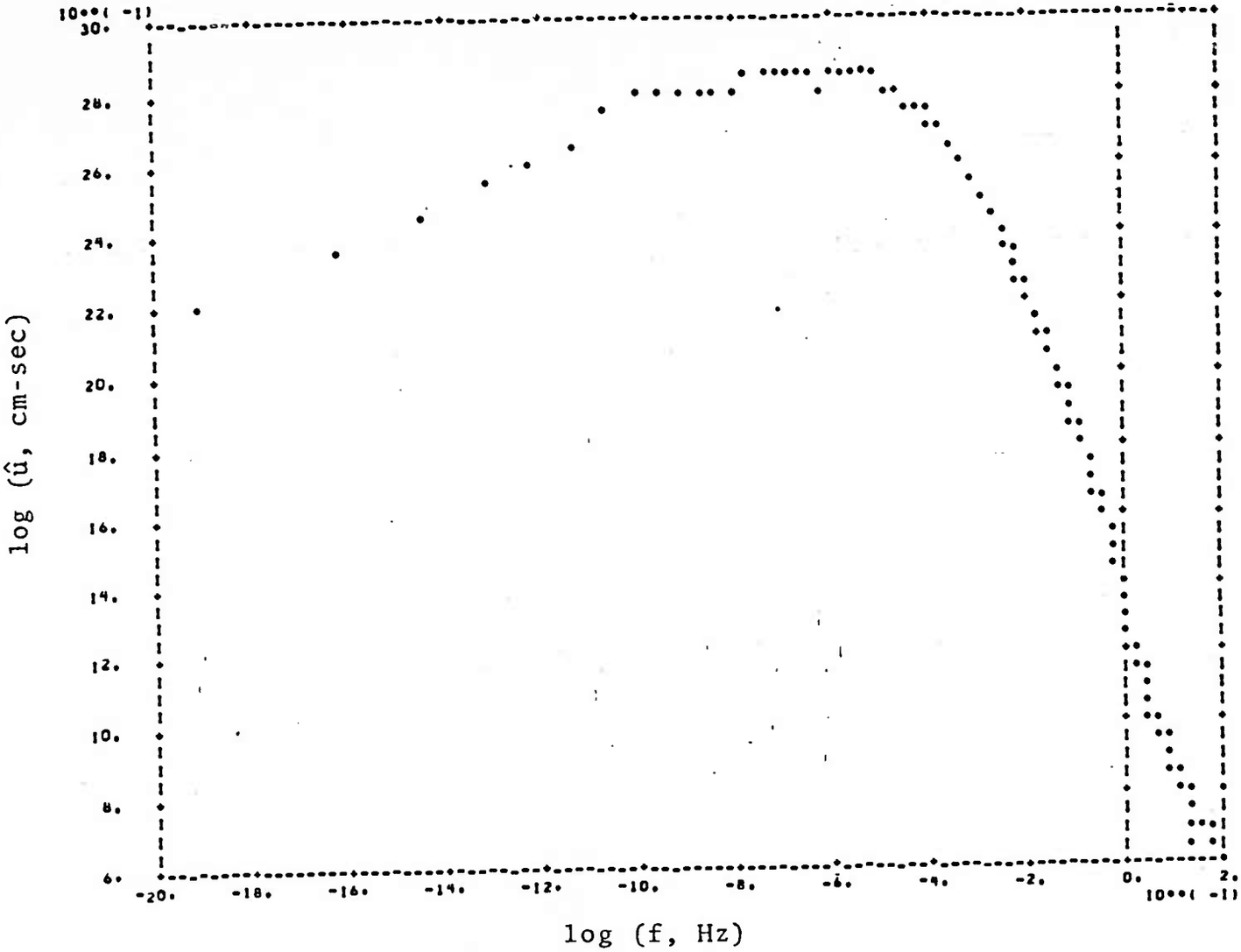

Fig. 38--Displacement spectrum for the horizontal component of ground motion at the epicenter for Calculation T-90. The station was 2.8 fault dimensions from the center of the fault.

REFERENCES

Allen, C. R., G. R. Enger, T. C. Hanks, J. M. Nordquist, and W. R. Thatcher, "Main Shock and Larger After-Shocks of the San Fernando Earthquake February 9 through March 1," U.S.G.S. Porf. Paper 733, 17-20, 1971.

Cherry, J. T., C. B. Archambeau, T. C. Bache, D. G. Harkrider, "The Teleseismic Radiation Field from Explosions: The Dependence of M_s and m_b on Earth Structure and Near Source Environment," Systems, Science and Software Report SSS-R-73-1834, August 22, 1973.

Hanks, Thomas C., "The Faulting Mechanism of the San Fernando Earthquake," Contribution No. 2346, Division of Geological and Planetary Sciences, California Institute of Technology, 1973.

Jungels, P. H., and G. A. Frazier, "Finite Element Analysis of the Residual Displacements for an Earthquake Rupture: Source Parameters for the San Fernando Earthquake," J. Geophys. Res. (to be published), 1973.

Whitcomb, J. H., C. R. Allen, J. D. Garmany, and J. A. Hileman, "The 1971 San Fernando Earthquake Series: Focal Mechanisms and Tectonics," Rev. Geophys. & Space Phys. (to be published) 1973.